J. metamorphic Geol., 2005, **23,** 511–531 doi:10.1111/j.1525-1314.2005.00591.x

Modelling of mineral equilibria in ultrahigh-temperature metamorphic rocks from the Anápolis–Itauçu Complex, central Brazil

J. A. BALDWIN,[1] R. POWELL,[2] M. BROWN,[1] R. MORAES[3] AND R. A. FUCK[4]
[1]*Laboratory for Crustal Petrology, Department of Geology, University of Maryland, College Park, MD 20742, USA (jbaldwin@geol.umd.edu)*
[2]*School of Earth Sciences, University of Melbourne, Parkville, Victoria 3052, Australia*
[3]*Instituto de Geociências, Universidade de São Paulo, São Paulo, Brazil*
[4]*Instituto de Geociências, Universidade de Brasília, Brasília, Brazil*

ABSTRACT A new quantitative approach to constraining mineral equilibria in sapphirine-bearing ultrahigh-temperature (UHT) granulites through the use of pseudosections and compatibility diagrams is presented, using a recently published thermodynamic model for sapphirine. The approach is illustrated with an example from an UHT locality in the Anápolis–Itauçu Complex, central Brazil, where modelling of mineral equilibria indicates peak metamorphic conditions of about 9 kbar and 1000 °C. The early formed, coarse-grained assemblage is garnet–orthopyroxene–sillimanite–quartz, which was subsequently modified following peak conditions. The retrograde pressure–temperature (*P–T*) path of this locality involves decompression across the FeO–MgO–Al_2O_3–SiO_2 (FMAS) univariant reaction orthopyroxene + sillimanite = garnet + sapphirine + quartz, resulting in the growth of sapphirine–quartz, followed by cooling and recrossing of this reaction. The resulting microstructures are modelled using compatibility diagrams, and pseudosections calculated for specific grain boundaries considered as chemical domains. The sequence of microstructures preserved in the rocks constrains a two-stage isothermal decompression–isobaric cooling path. The stability of cordierite along the retrograde path is examined using a domainal approach and pseudosections for orthopyroxene–quartz and garnet–quartz grain boundaries. This analysis indicates that the presence or absence of cordierite may be explained by local variation in a_{H_2O}. This study has important implications for thermobarometric studies of UHT granulites, mainly through showing that traditional FMAS petrogenetic grids based on experiments alone may overestimate *P–T* conditions. Such grids are effectively constant a_{H_2O} sections in FMAS-H_2O (FMASH), for which the corresponding a_{H_2O} is commonly higher than that experienced by UHT granulites. A corollary of this dependence of mineral equilibria on a_{H_2O} is that local variations in a_{H_2O} may explain the formation of cordierite without significant changes in *P–T* conditions, particularly without marked decompression.

Key words: a_{H_2O}; Brazil; cordierite; pseudosection; sapphirine; THERMOCALC; UHT metamorphism.

INTRODUCTION

Determining the pressure–temperature (*P–T*) paths of metamorphic rocks is essential for placing constraints on tectonic models of orogenic processes. Constraining maximum *P–T* conditions is particularly important for ultrahigh-temperature (UHT) granulites, which record extreme temperatures (> 900 °C) at moderate crustal pressures (7–13 kbar). Assemblages such as sapphirine coexisting with quartz and aluminous orthopyroxene coexisting with sillimanite and quartz are diagnostic mineral assemblages for UHT metamorphism of aluminous supracrustal rocks. The reality that crustal rocks are subjected to such extreme temperatures has important implications for constraining the tectonic scenarios under which such *P–T* conditions may be achieved. Thus, evaluating the peak *P–T* conditions and retrograde histories of UHT granulites is essential to the evaluation of tectonic and thermal models for the formation and evolution of high-grade terranes (Bohlen, 1987, 1991; Harley, 1989; Sandiford & Powell, 1991; Brown, 2002).

The ability to place quantitative constraints on the *P–T* evolution of UHT granulites has historically been limited by (1) the inability of cation-partitioning thermometers to record peak temperature conditions (Frost & Chacko, 1989; Fitzsimons & Harley, 1994; Pattison & Begin, 1994; Pattison *et al.*, 2003), and (2) the lack of an adequate thermodynamic model for sapphirine in the FeO–MgO–Al_2O_3–SiO_2 (FMAS) system, which prevented the incorporation of sapphirine into internally consistent thermodynamic data

sets. Typically, quantitative experimental and semi-quantitative *P–T* projections depicting univariant reactions and divariant equilibria have been applied to constrain the *P–T* evolution of sapphirine-bearing granulites in various model systems (Hensen, 1971, 1986; Harley, 1989, 1998a; Hensen & Harley, 1990; Bertrand *et al*., 1991; Audibert *et al*., 1995; Carrington & Harley, 1995a,b; Brown & Raith, 1996; Raith *et al*., 1997; Harley & Motoyoshi, 2000; McDade & Harley, 2001; Hollis & Harley, 2003).

Hensen (1971) adopted the concept of equilibrium phase diagrams within a defined bulk compositional system in order to explore the stability of garnet–cordierite parageneses in metapelites. These diagrams, now known informally as pseudosections, are generally constructed in terms of two intensive variables (e.g. *P* & *T*) or an intensive and an extensive variable (e.g. *T* & *V*) (Powell *et al*., 2005). A pseudosection approach to evaluating mineral assemblage stability in a rock provides a quantitative method for interpreting the *P–T* evolution of a sample, as this approach accounts for both bulk composition and multivariant equilibria. This forward modelling approach has revealed that univariant reactions are only sometimes intersected by individual rocks of specified bulk composition, thereby limiting the usefulness of projections that depict only univariant equilibria. In recent years, internally consistent thermodynamic data sets have been expanded to include a broader range of end-members of phases, allowing for modelling that more closely approximates natural systems (Holland & Powell, 1998; White *et al*., 2001; Johnson *et al*., 2003a; Johnson & Brown, 2004). Additionally, exploration of different combinations of variables (e.g. *P*, *T*, *X* & a_{H_2O}) reveals information about processes such as fluid infiltration, melt loss and scales of equilibrium (Guiraud *et al*., 2001; White & Powell, 2002; Powell *et al*., 2005).

The pseudosection approach has been successfully applied to evaluate the evolution of stable mineral assemblages in metapelitic rocks (e.g. Tinkham *et al*., 2001; White *et al*., 2002; Boger & White, 2003; Johnson *et al*., 2003b; Kelsey *et al*., 2003; Johnson & Brown, 2004), but this approach has only recently been made possible for studies of UHT granulites by the work of Kelsey *et al*. (2004), which provided a new activity–composition (*a–X*) model for sapphirine. This model allows for consistent phase diagram calculations and thus a more quantitative assessment of the metamorphic evolution of UHT granulite terranes than has previously been possible. Historically, mineral assemblages and reaction microstructures in sapphirine–quartz and orthopyroxene–sillimanite–quartz granulites in the $FeO–MgO–Al_2O_3–SiO_2–H_2O$ (FMASH) model system have been evaluated to characterize UHT metamorphism (Harley, 1985; Harley *et al*., 1990; Harley & Hensen, 1990; Brown & Raith, 1996; Ouzegane & Boumaza, 1996; Raith *et al*., 1997; Harley & Motoyoshi, 2000; Moraes *et al*., 2002; Kelsey *et al*., 2003, 2004; Ouzegane *et al*., 2003). Petrogenetic grids involving equilibria in the FMAS(H) system have been used qualitatively to suggest the overall shape of *P–T* paths based on arrested reaction microstructures (e.g. symplectites, coronae) (e.g. Harley *et al*., 1990; Ouzegane & Boumaza, 1996; Harley, 1998b).

In this study, phase relationships were modelled using THERMOCALC (Powell & Holland, 1988; Holland & Powell, 1998; Powell *et al*., 1998), with the recently published *a–X* model for sapphirine (Kelsey *et al*., 2004 for calculations in the FMAS(H) system. However, this study goes beyond the simple determination of the shape of the *P–T* path in terms of decompression and/or cooling and in particular uses domainal equilibrium (e.g. Harley *et al*., 1990; Harley, 1998a) to evaluate individual microstructures that each evolve as separate compositional domains. The study demonstrates that by using this approach, phase diagrams for each domain may be constructed and compared with one another in order to constrain the *P–T* evolution of the rock more accurately. Mineral assemblages and mineral reaction sequences of an UHT granulite locality in the Anápolis–Itauçu Complex (AIC), central Brazil, are evaluated using this approach. An important conclusion is that the microstructures may be consistently explained by the same slight changes in *P* and/or *T* during the evolution of the rock, and do not require large degrees of decompression and/or cooling that might be implied based on a more qualitative approach.

PHASE RELATIONS IN FMAS(H)

Methods that have been applied historically to interpret the evolution of mineral assemblages in UHT sapphirine-bearing assemblages include the use of the univariant reactions or divariant equilibria that lie within the FMAS or KFMASH systems (Hensen, 1971; Hensen & Green, 1973; Harley, 1998a). Kelsey *et al*. (2004) observed that a comparison of the published experimental and calculated grids reveals a significant discrepancy. The position of the invariant points in FMAS, which has been the subject of considerable debate in previous studies, is not in agreement in a comparison of experimentally derived and calculated petrogenetic grids. In the Kelsey *et al*. (2004) study, these invariant points lie within a 950–1000 °C window around 6.5 kbar (Fig. 1a), whereas other studies in the literature place them at higher pressure, between 7.5 and 10.5 kbar (Hensen, 1971; Hensen & Green, 1973; Harley, 1998a) (see fig. 1c of Kelsey *et al*., 2004).

In particular, the position of the spinel-absent [Spl] invariant point is of interest because the univariant reactions around this point have been used to constrain the *P–T* stability of sapphirine–quartz and orthopyroxene–sillimanite–quartz UHT assemblages. Hensen & Green (1973) placed this point at 9.5 ± 1 kbar and 1030 °C, Harley (1998a) placed it

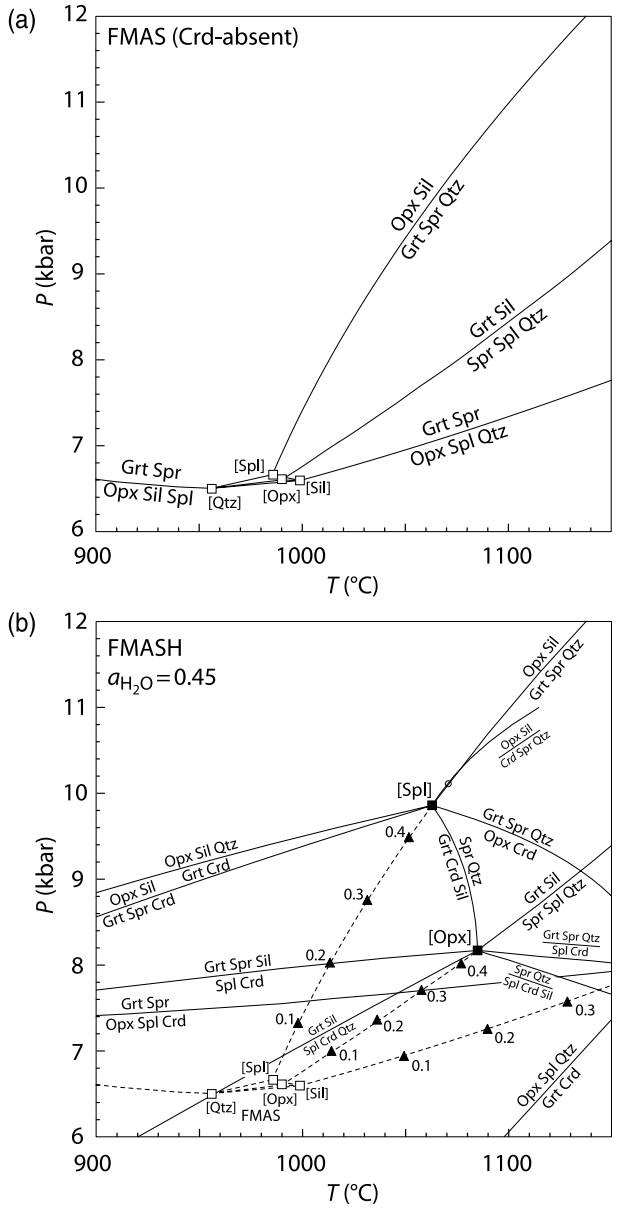

Fig. 1. *P–T* diagrams for the FMAS and FMASH systems. (a) Cordierite-absent (dry) FMAS equilibria. (b) Constant a_{H_2O} FMASH projection for $a_{H_2O} = 0.45$. The triangles indicate position of FMASH invariant points at specified values of a_{H_2O}. These are located at higher temperatures than the FMAS invariant points along the cordierite-absent univariant reactions in FMAS (dashed lines). Compare to fig. 1c of Kelsey *et al.* (2004). The inconsistency between the calculated FMAS invariant points and the experimentally and qualitatively derived equilibria may be explained by the presence of impurities in the experimental charges. This does not allow for the determination of true (dry) FMAS equilibria and in effect such grids may represent constant a_{H_2O} sections (around 0.35 for Hensen, 1971; Hensen & Green, 1973 and around 0.45 for Harley, 1998a). Abbreviations after Kretz (1983).

at 10.2 kbar and 1050 °C, and Kelsey *et al.* (2004) calculated it at 6.7 kbar and 990 °C (Fig. 1). Kelsey *et al.* (2004) concluded that the difference most likely reflects the presence of a small amount of water in the experimental charges, so that the experiments relate to FMASH equilibria, and not FMAS equilibria. The water results in a displacement of the 'FMAS' [Spl] invariant point to higher pressure along the corresponding cordierite-absent FMASH reaction that stems from the actual [Spl] FMAS invariant point at lower pressure (Fig. 1). At high *P–T* along this reaction hydrous melt is eventually introduced at an FMASH invariant point (Fig. 1). The often-applied Harley (1998a) grid is similar to a constant a_{H_2O} section in FMASH at about $a_{H_2O} = 0.45$ (Fig. 1b). If the a_{H_2O} of rocks in the granulite facies is generally less than this value (Yardley & Valley, 1997), as we argue at least for the following example, then peak pressures and temperatures will be overestimated using the Harley (1998a) grid. Thus, the absolute *P–T* and *P–T* evolution for UHT granulites in which metamorphic conditions have been determined based on the Harley (1998a) grid should be re-evaluated.

A complication is the role of the CO_2 found along with H_2O in natural cordierite (Harley *et al.*, 2002), and its presence may also stabilize cordierite in the larger system, FMASH + CO_2. Although a grid for this system has not been calculated yet, it is anticipated that the effect of CO_2 will be similar to that of H_2O, with cordierite-bearing equilibria extending to higher pressure as a_{CO_2} increases (at fixed a_{H_2O}).

THE ANÁPOLIS–ITAUÇU COMPLEX, CENTRAL BRAZIL

Geological setting

The Neoproterozoic Brasília Fold Belt (BFB) displays tectonic elements that developed due to ocean basin closure, arc-continent collision, and, in the northern BFB, collision between the Goiás Magmatic Arc to the west and the São Francisco Craton to the east (Fig. 2a) (Pimentel *et al.*, 2000). The BFB extends over 1100 km north–south from south-eastern Tocantins through Goiás, to western Minas Gerais. The BFB is one of the best-preserved orogenic belts in Brazil, displaying features such as ophiolitic mélange, calc-alkaline arc rocks, S-type collisional granites, and regional-scale nappe systems indicating tectonic transport to the east (Pimentel *et al.*, 2000).

The eastern, external zone of the BFB comprises several sedimentary and metasedimentary units that are progressively more deformed and metamorphosed to the west. The Araxá Group, which is composed predominantly of turbidite-type sediments, volcanic rocks, and ophiolitic mélange, is part of the internal zone. To the west, is an aerially extensive Neoproterozoic juvenile arc, the Goiás magmatic arc, comprising volcano-sedimentary rocks and tonalite and granodiorite gneisses. Arc magmatism began *c.* 930–900 Ma and pre-collisional calc-alkaline magmatism lasted until *c.* 640 Ma (Pimentel *et al.*, 2000).

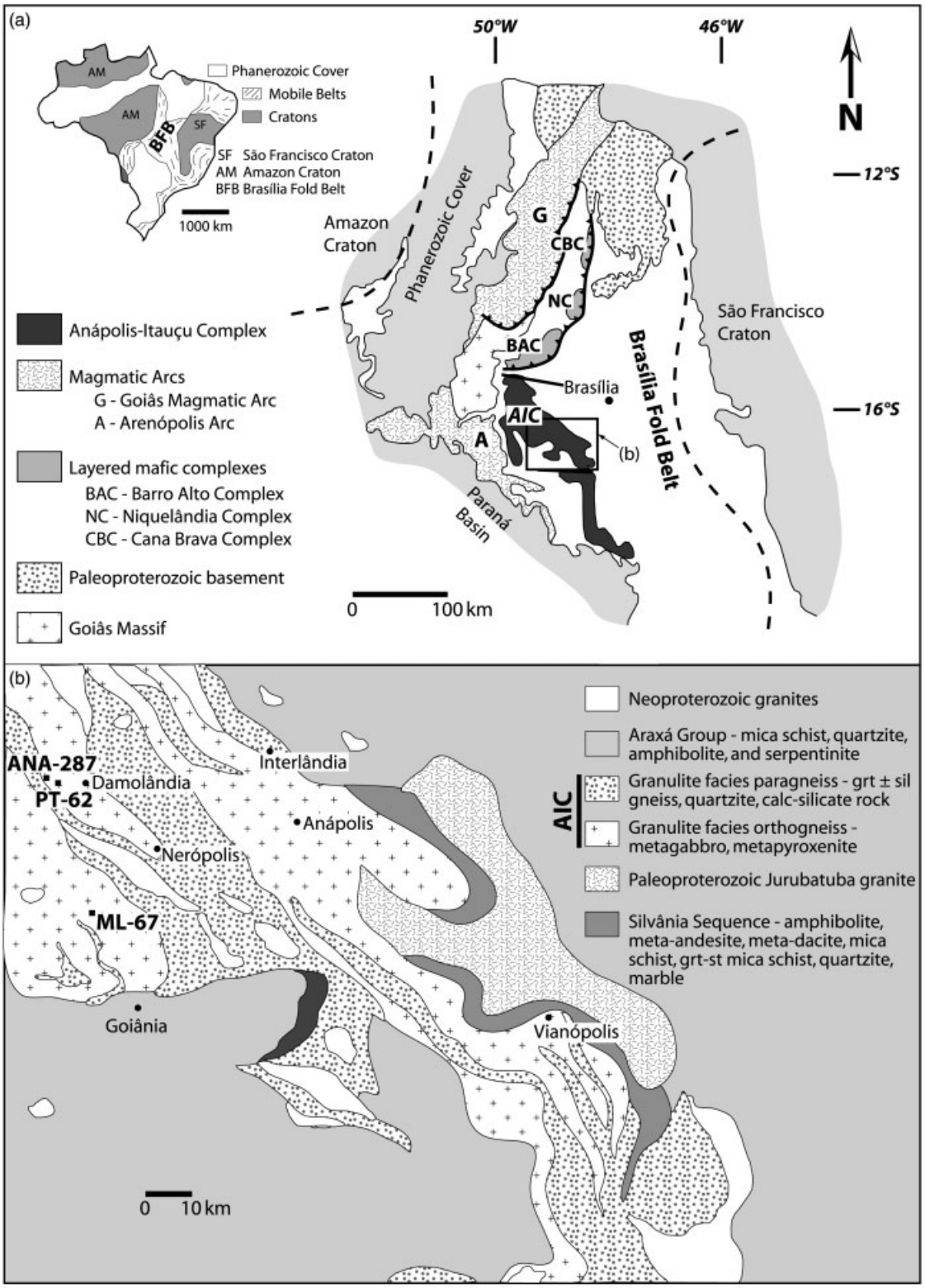

Fig. 2. (a) Geological map of Brasília Fold Belt showing the location of the Anápolis–Itauçu Complex and the surrounding units (after Pimentel *et al.*, 2004). Dashed lines indicate craton extent. Box outlines area shown in (b). Inset shows map of Brazil with the location of the Brasília Fold Belt. (b) Geological map of the Anápolis–Itauçu Complex showing the location of the study area. UHT granulites have been identified at three localities: ML-67, PT-62 and ANA-287 (Moraes *et al.*, 2002). The samples discussed in this study are from locality ML-67 of Moraes *et al.* (2002). Modified from Piuzana *et al.* (2003).

The AIC forms an NNW-oriented terrane (260 km × 70 km) of predominantly granulite facies rocks in the south–central core internal zone of the BFB (Fig. 2b). The AIC is bounded on the west and east by mylonite zones separating the AIC from greenschist to amphibolite facies rocks of the Araxá Group and, in the westernmost extent of the complex, the Goiás magmatic arc. The AIC comprises (1) an orthogneiss unit derived from tonalite, granodiorite and mafic–ultramafic layered bodies, and (2) a paragneiss unit, including aluminous granulite, garnet–sillimanite gneiss, calc-silicate rocks, marble and quartzite. Other lithologies include volcanosedimentary sequences and a large number of elongate, NW–SE-oriented granitoid intrusions. Recent geochronological data from the AIC indicate that magmatism and metamorphism occurred *c*. 650–630 Ma, related to final ocean closure between the São Francisco and Amazonian continents (Piuzana *et al*., 2003; Pimentel *et al*., 2004).

UHT granulites in the AIC have been identified at three localities (Fig. 2b) (Moraes *et al*., 2002). North of Goiânia (locality ML-67 of Moraes *et al*., 2002), an impure quartzite preserves sapphirine–quartz and aluminous orthopyroxene–sillimanite–quartz assemblages. Moraes *et al*. (2002) concluded that high Al_2O_3 in orthopyroxene (12.9 wt%) combined with a lack of cordierite in the samples they studied and development of late biotite constrained the metamorphic evolution of this sample from *P–T* conditions of >1150 °C at >10 kbar by near-isobaric cooling to temperatures around 900 °C.

Near Damolândia (locality PT-62 of Moraes *et al*., 2002), sapphirine occurs in both quartz-rich and quartz-poor rocks. In the sapphirine-bearing, quartz-poor rock, the peak mineral assemblage is inferred to have been orthopyroxene–garnet–sillimanite–quartz. Moats of cordierite surround garnet and symplectites of sapphirine–cordierite–plagioclase and spinel–cordierite–plagioclase surround sillimanite. Garnet rims were subsequently replaced by three orthopyroxene-bearing symplectites, with sapphirine, spinel, or cordierite, respectively. Subsequently, orthopyroxene–sapphirine symplectites are interpreted to have reacted with melt to produce granular intergrowths of cordierite–spinel–biotite. In the quartz-rich sapphirine-bearing rock, the peak mineral assemblage reflects the reaction of orthopyroxene–quartz–sillimanite to garnet–sapphirine. Garnet rims were replaced by coronae of orthopyroxene–cordierite.

In a third locality at the Monjolo Stream, approximately 3 km west of the Damolândia locality (locality ANA-287 of Moraes *et al*., 2002), sapphirine-absent metapelitic rocks contain aluminous (Al_2O_3 of 9.7 wt%) orthopyroxene together with cordierite–sillimanite–spinel intergrowths, which may record sapphirine breakdown. A composite post-thermal peak *P–T* path from the Damolândia and Monjolo stream localities, based on the observed microstructural relations and mineral reaction sequences, was interpreted to have involved a decompression segment from >12 to <8 kbar at 1100–1000 °C, followed by near-isobaric cooling from 1000 to <600 °C at <8 to <6 kbar (Moraes *et al*., 2002).

Moraes *et al*. (2002) concluded that after the metamorphic peak, the *P–T* path for both areas followed a near-isobaric cooling stage to <900 °C; however, based on the absence of cordierite at the ML-67 locality, these two paths were interpreted to be separated by about 3 kbar. This led Moraes *et al*. (2002) to suggest oblique exhumation of an isothermal lower crustal section.

Petrography and mineral chemistry

Sample description

The samples used in this study to illustrate the modelling methodology are from locality ML-67 of Moraes *et al*. (2002) (Fig. 2b), where an impure quartzite contains a compositional layering defined by differing proportions of quartz, orthopyroxene, garnet and sillimanite, and exhibits a pervasive foliation. The outcrop apparently occurs as isolated blocks within 'common' orthopyroxene granulite. Because of very poor exposure, structural relationships between the UHT granulites and the surrounding rocks are not known in any greater detail.

Garnet (1–5 mm) and orthopyroxene (5–15 mm) porphyroblasts occur, with laths of smaller sillimanite set in a matrix of mm-size quartz (Fig. 3a,b). Orthopyroxene porphyroblasts invariably contain needles of sillimanite (Fig. 3c), and, less commonly, inclusions of 1–3 mm euhedral garnet at the rims of porphyroblasts (Fig. 3d). Sapphirine, which constitutes $<1\%$ of the mineral mode, occurs as small, prismatic crystals (<100 to 500 μm in length) (Fig. 3e), and as anhedral grains formed at the expense of the porphyroblast minerals, including garnet, orthopyroxene, sillimanite and cordierite (Fig. 3f–k). Sapphirine, quartz and sillimanite occur as composite inclusion microstructures in porphyroblastic garnet cores (Fig. 3g–i). Sapphirine inclusions in orthopyroxene are commonly separated from the orthopyroxene by a thin rim of sillimanite (Fig. 3f).

New sampling in 2003 reveals that cordierite does occur sporadically in the ML-67 locality, in contrast to the original sample set of Moraes *et al*. (2002). It commonly nucleates around sillimanite, and rims both orthopyroxene and garnet (Fig. 3j–l). Scarce plagioclase occurs as inclusions in garnet. K-feldspar has not been observed in these samples. Biotite occurs as an additional phase, defining the fabric along with less aluminous orthopyroxene. Accessory phases include zircon, monazite, rutile, ilmenite and pyrite.

Mineral chemistry

Chemical compositions of minerals were obtained on the JEOL JXA-8900 Superprobe at the University

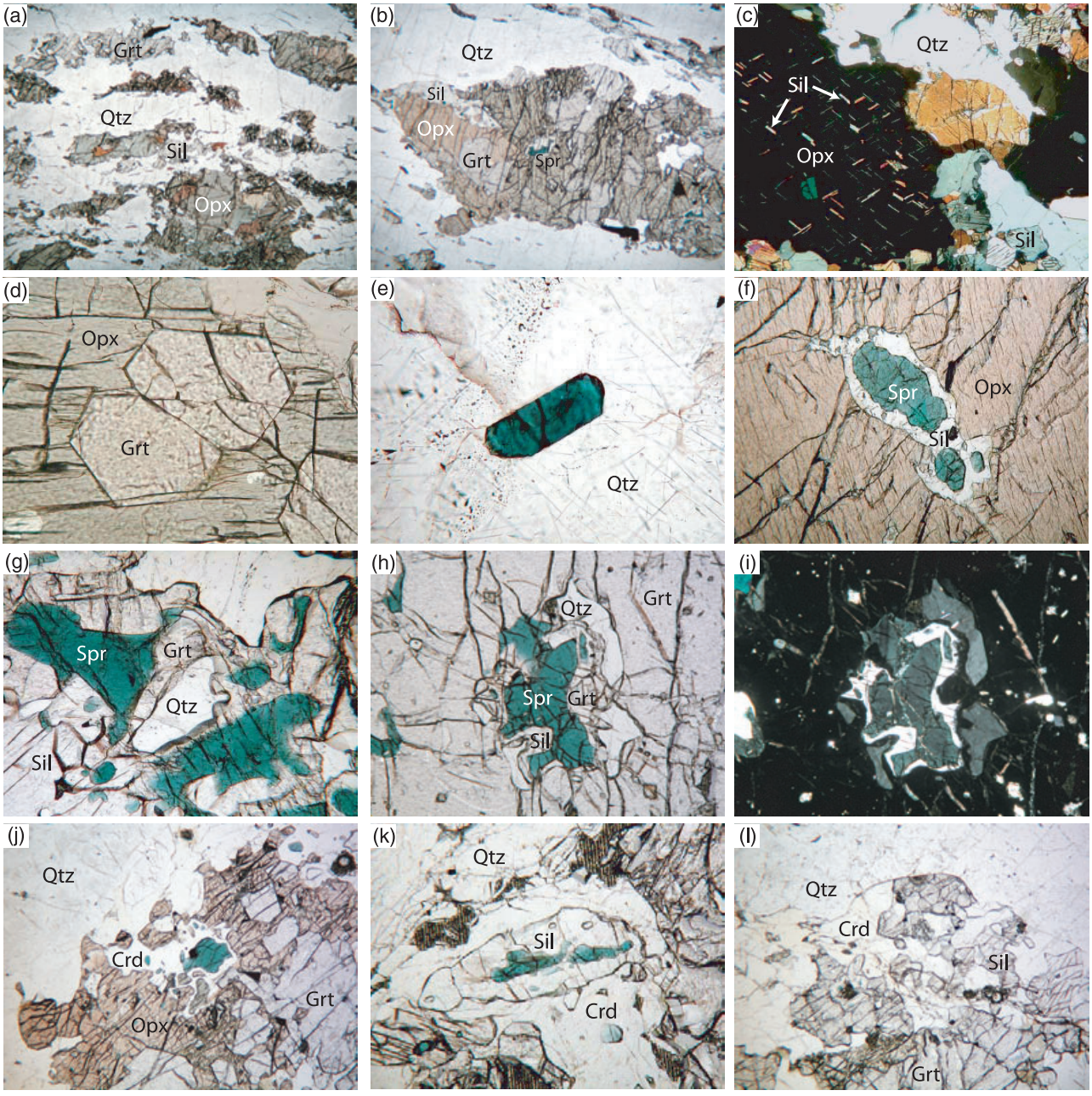

Fig. 3. Photomicrographs from locality ML-67 to illustrate microstructures in UHT granulites of the Anápolis–Itauçu Complex. (a) Primary assemblage of garnet, orthopyroxene, sillimanite and quartz. Elongate garnet porphyroblasts. Sillimanite occurs at the rim of orthopyroxene. Plane-polarized light, long dimension is 12 mm. (b) Peak assemblage of garnet–orthopyroxene–sillimanite–quartz. Sapphirine inclusion in orthopyroxene is rimmed by sillimanite. Garnet inclusions in orthopyroxene. Plane-polarized light, long dimension is 5 mm. (c) Orthopyroxene porphyroblast with needle-like inclusions of sillimanite. Crossed-polarized light, long dimension is 4 mm. (d) Euhedral garnet inclusions in orthopyroxene. Plane-polarized light, long dimension is 0.9 mm. (e) Euhedral inclusion of sapphirine in quartz. Plane-polarized light, long dimension is 0.8 mm. (f) Sapphirine inclusion in orthopyroxene. Rim of sillimanite separates sapphirine from orthopyroxene. Plane-polarized light, long dimension is 1.8 mm. (g) Sapphirine and quartz inclusions in garnet. Former sapphirine–quartz grain boundaries are now separated by rim of garnet or sillimanite. Sillimanite is adjacent to sapphirine in lower left quadrant. Plane-polarized light, long dimension is 1.5 mm. (h) Sapphirine and quartz inclusions in garnet separated by garnet and sillimanite. Garnet occurs adjacent to quartz and sillimanite occurs adjacent to sapphirine. Plane-polarized light, long dimension is 2 mm. (i) Same as (h) in crossed-polarized light showing thin rim of garnet between quartz and sillimanite. Long dimension is 2 mm. (j) Cordierite and orthopyroxene at rim of garnet. Sapphirine occurs as inclusions in cordierite. Euhedral garnet in orthopyroxene in upper centre field of view. Plane-polarized light, long dimension is 3 mm. (k) Sapphirine rimmed by sillimanite included in cordierite at edge of garnet. Plane-polarized light, long dimension is 1.6 mm. (l) Cordierite at edge of garnet shown in Fig. 4. Cordierite nucleates around sillimanite. Plane-polarized light, long dimension is 3.5 mm.

of Maryland. For elemental mapping, operating conditions were 15 kV and 30–100 nA. For spot chemical analyses, operating conditions were 15 kV and 20–30 nA. A selection of representative mineral compositions is given in Table 1. H_2O and CO_2 contents of cordierite were measured *in-situ* by SIMS, on the Cameca IMS-4f ion microprobe at the Grant Institute of Earth Science, University of Edinburgh. Analysis was carried out following the procedures and analytical conditions described by Harley *et al*. (2002). Sapphirine was analysed for Be also using the IMS-4f at Edinburgh.

Primary *garnet* occurs as 1–5 mm porphyroblasts that are sometimes elongate within the foliation; it is mainly pyrope-almandine, with $X_{Mg} = Mg/(Mg + Fe^{2+}) = 0.59–0.61$ and contains inclusions of sillimanite, sapphirine and quartz. These inclusions may be monomineralic or may occur as complex reaction microstructures. For example, sillimanite sometimes occurs as composite inclusions in which the sillimanite is rimmed by anhedral grains of sapphirine and quartz separating sillimanite and garnet (Figs 3g & 4a–c). Sapphirine occurs adjacent to sillimanite with quartz outboard adjacent to garnet. A thin rim of secondary garnet with the same composition as the primary garnet, or of sillimanite, commonly occurs between sapphirine and quartz (Figs 3g–i & 4b,c). Additional secondary garnet occurs as small (< 1 mm), euhedral inclusions within orthopyroxene porphyroblasts, with $X_{Mg} = 0.54$.

Orthopyroxene has a high alumina content (12.9–10.5 wt% Al_2O_3 in the cores; $y_{Opx} = X^{Opx}_{Al,M1} = 0.24–0.20$) and X_{Mg} ranging from 0.72 to 0.69 (Table 1). A significant decrease in alumina occurs at the rim of porphyroblasts (9.5–7.5 wt% Al_2O_3; $y_{Opx} = 0.18–0.15$). Secondary orthopyroxene occurs as rims on garnet porphyroblasts (Fig. 4d,e), with alumina content similar to the rim compositions of the primary porphyroblasts (9.8–7.6 wt% Al_2O_3; $y_{Opx} = 0.18–0.15$). Orthopyroxene within the foliation has Al_2O_3 contents similar to rim compositions of primary orthopyroxene.

Sapphirine is uniform in composition regardless of its petrographic setting ($X_{Mg} = 0.81–0.78$; Be = 5 ppm). It occurs in reaction microstructures, as described above, as well as monomineralic inclusions associated with all of the major porphyroblasts – garnet, orthopyroxene and sillimanite. Most commonly, inclusions in garnet and orthopyroxene are rimmed by a thin moat of sillimanite.

Cordierite is scarce in these rocks and nucleates around preexisting sillimanite porphyroblasts at the rims of garnet and orthopyroxene (Figs 3j–l, 4d,e & 5). Cordierite is uniform in composition and is Mg-rich, with $X_{Mg} = 0.90$ (Table 1), and contains 0.87 wt% H_2O and 1.44 wt% CO_2.

Mineral assemblage evolution

Diagnostic UHT mineral assemblages at the ML-67 locality include sapphirine–quartz and aluminous orthopyroxene–sillimanite–quartz. Based on the petrographic evidence presented above, particularly the porphyroblastic nature of garnet, orthopyroxene and silimanite, the oldest UHT mineral assemblage at this locality is inferred to be garnet–orthopyroxene–

Table 1. Representative electron microprobe analyses from ML-67 locality.

	Garnet						Orthopyroxene				Sapphirine		Cordierite
Weight %	C	C (S-Q)	R (Qtz)	R (Crd)	R (Opx)	EI (Opx)	C (Grt)	R (Grt)	C (P)	R (P)	C (Grt)	R (Grt)	Adj Grt
SiO_2	41.14	40.99	40.78	40.47	40.18	40.58	49.80	50.52	47.08	49.23	14.30	14.08	50.18
TiO_2	0.03	0.01	0.02	0.01	0.01	0.03	0.23	0.22	0.20	0.14	0.08	0.06	0.01
Al_2O_3	22.67	22.77	22.75	22.42	23.35	22.46	9.60	8.66	12.28	9.64	59.39	61.59	34.46
Cr_2O_3	0.01	bd	0.01	bd	0.01	bd	bd	bd	0.02	0.01	0.01	0.00	
FeO	18.35	18.73	18.19	20.07	20.31	21.01	16.21	15.91	16.92	17.02	10.06	7.45	2.42
MnO	1.24	1.23	1.34	1.40	1.47	1.53	0.35	0.32	0.49	0.46	0.15	0.14	0.05
MgO	15.88	15.60	15.70	14.35	13.93	13.77	24.67	25.20	22.92	23.92	16.66	16.69	11.74
CaO	0.95	0.89	0.97	1.00	0.90	0.93	0.04	0.04	0.08	0.06	0.01	0.00	0.01
Na_2O							bd	bd	bd	0.01	0.01	0.00	0.12
Total	100.28	100.22	99.74	99.71	100.17	100.32	100.91	100.87	99.99	100.49	100.66	100.02	98.99
Si	3.02	3.02	3.01	3.02	2.98	3.02	1.78	1.80	1.70	1.77	0.85	0.84	4.99
Ti	0.00	0.00	0.00	0.00	0.00	0.00	0.01	0.01	0.01	0.00	0.00	0.00	0.00
Al	1.96	1.97	1.98	1.97	2.04	1.97	0.40	0.36	0.52	0.41	4.12	4.31	4.04
Cr	0.00	0.00	0.00	0.00	0.00	0.00	0.00	0.00	0.00	0.00	0.00	0.00	
Fe^{2+}	1.13	1.12	1.12	1.25	1.26	1.31	0.46	0.46	0.45	0.48	0.37	0.36	0.20
Fe^{3+}							0.03	0.02	0.06	0.04	0.13	0.02	
Mn	0.08	0.08	0.08	0.09	0.09	0.10	0.01	0.01	0.02	0.01	0.01	0.01	0.00
Mg	1.74	1.71	1.73	1.59	1.54	1.53	1.31	1.34	1.24	1.28	1.48	1.48	1.74
Ca	0.08	0.07	0.08	0.08	0.07	0.07	0.00	0.00	0.00	0.00	0.00	0.00	0.00
Na							0.00	0.00	0.00	0.00	0.00	0.00	0.02
Total	8.00	8.00	8.00	8.00	8.00	8.00	4.00	4.00	4.00	4.00	7.00	7.00	11.00
X_{Mg} (all Fe^{2+})	0.61	0.60	0.61	0.56	0.55	0.54	0.73	0.74	0.71	0.71	0.75	0.80	0.90
X_{Mg} (with Fe^{3+})							0.74	0.75	0.73	0.73	0.80	0.81	
y_{Opx}							0.18	0.17	0.23	0.18			

bd, Below detection; C, core; R, rim; EI, euhedral inclusion; P, porphyroblast; S-Q, Spr-Qtz; $y_{Opx} \equiv X^{Opx}_{Al,M1}$. ( ) indicate mineral adjacent or included within.

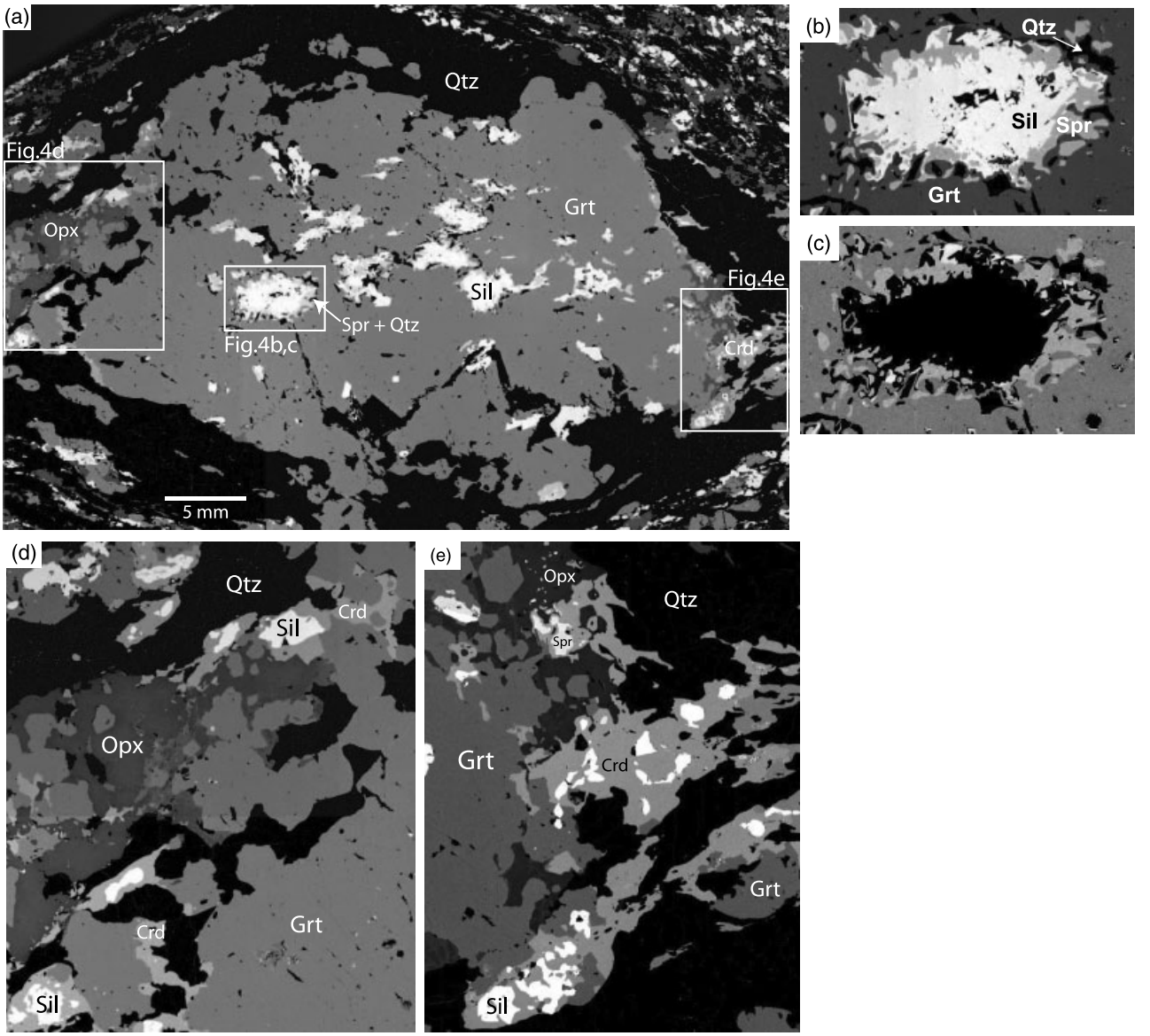

Fig. 4. X-ray compositional maps from ML-67. (a) Al X-ray map. Large garnet porphyroblast surrounded by ribbon quartz matrix. Garnet contains inclusions of sillimanite that are rimmed by sapphirine–quartz. Garnet is rimmed by secondary orthopyroxene and cordierite. Boxes indicate locations of (b)–(e). (b) Al X-ray map of sillimanite inclusion in garnet. Reaction microstructure of sapphirine–quartz surrounds sillimanite indicating the divariant reaction Grt + Sil = Spr + Qtz. Garnet replaces former grain-boundary contacts between sapphirine and quartz. (c) Mg X-ray compositional map of inclusion shown in (b). (d) Al X-ray compositional map. Left edge of large garnet in (a) showing cordierite and orthopyroxene rimming garnet. Cordierite nucleates around preexisting sillimanite crystals. Note small euhedral garnet included in orthopyroxene at left centre edge of image. (e) Right edge of garnet shown in (a). Cordierite nucleates around sillimanite and sapphirine. Note euhedral garnet included in orthopyroxene in top left field of view.

sillimanite–quartz and that sapphirine–quartz formed as a secondary mineral assemblage. Evidence for this is given by the composite reaction microstructures formed around sillimanite inclusions in garnet, which indicate a reaction of garnet and sillimanite to produce sapphirine and quartz. The coarse-grained assemblage garnet–orthopyroxene–sillimanite–quartz is henceforth referred to as the peak assemblage, by which we mean the assemblage that records the earliest metamorphic conditions in the rock. It provides the starting point of the *P–T* path that can be determined from the rocks in our modelling of mineral equilibria.

Following peak conditions during which the porphyroblast phases in the rock are interpreted to have been in equilibrium with each other, the rock developed into domains where microstructures involving

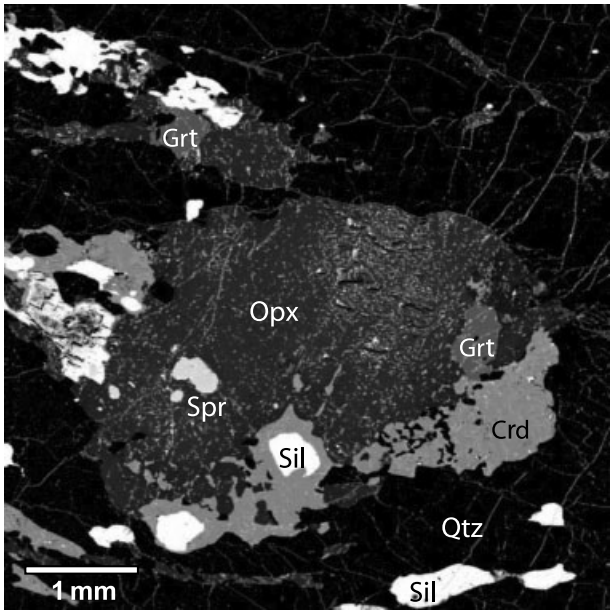

Fig. 5. Al X-ray compositional map of orthopyroxene porphyroblast in quartz matrix. Orthopyroxene contains inclusions of garnet and sapphirine and is rimmed by sillimanite and cordierite. Cordierite occurs between former grain boundaries of orthopyroxene–quartz–sillimanite indicating the reaction Opx + Sil + Qtz = Grt + Crd.

coronitic and symplectitic growth of secondary phases occurred. Three domains may be defined based on microstructures between minerals: garnet–sillimanite, garnet–quartz, and orthopyroxene–quartz. A domainal composition may be defined based on specified mineral proportions and measured mineral chemistry within a particular grain-boundary domain. The phase relations and important microstructures of each of these domains are discussed separately below.

Grain-boundary microstructural domains

Domain 1: Garnet–sillimanite. Sillimanite commonly occurs as inclusions in garnet with anhedral grains of sapphirine and quartz separating sillimanite and garnet (Figs 3g & 4a–c). Sapphirine tends to occur adjacent to sillimanite with quartz outboard adjacent to garnet. This microstructure records progress of the FMAS-divariant reaction,

$$\mathrm{Grt} + \mathrm{Sil} = \mathrm{Spr} + \mathrm{Qtz}, \quad (1)$$

following the crossing of the univariant reaction,

$$\mathrm{Opx} + \mathrm{Sil} = \mathrm{Grt} + \mathrm{Spr} + \mathrm{Qtz}, \quad (2)$$

across which the peak mineral assemblage of garnet–orthopyroxene–sillimanite–quartz had became unstable (cf. Moraes *et al*., 2002).

The thin rim of secondary garnet or sillimanite that occurs between sapphirine and quartz (Figs 3g & 4b,c) indicates that garnet and sillimanite were first consumed by crossing reaction (1) from left to right, followed by regrowth of garnet or sillimanite recording recrossing of reaction (1) from right to left. Similar relationships are seen where either the sillimanite inclusion has been consumed, or where the edge of an original sillimanite inclusion is intersected (Fig. 3h,i).

Domain 2: Garnet–quartz. Garnet porphyroblasts commonly exhibit euhedral sillimanite around the rim, and are surrounded by a quartz matrix (Fig. 4a). Sillimanite is typically isolated from garnet by a rim of cordierite indicating that Grt + Sil + Qtz may have initially reacted to form cordierite, thus isolating sillimanite from further reaction (Fig. 4d,e). Further reaction of garnet and quartz produced orthopyroxene and additional cordierite. The presence of some straight grain edges of garnet against orthopyroxene suggests garnet regrowth, either as new grains, or by grain-edge straightening of previously replaced garnet (Fig. 4d,e).

Domain 3: Orthopyroxene–quartz. In this domain, sillimanite is located at rims of orthopyroxene porphyroblasts, with cordierite nucleating around sillimanite (Fig. 5). Euhedral garnet occurs as inclusions near the rim of porphyroblastic orthopyroxene (Fig. 3d).

Modelling of mineral equilibria

Phase relations were modelled in the Na_2O–CaO–K_2O–FeO–MgO–Al_2O_3–SiO_2–H_2O (NCKFMASH) and FMAS(H) systems using THERMOCALC v.3.23 (Powell & Holland, 1988), and the data set of Holland & Powell (1998, version 5.5s, Nov. 2003), with the activity–composition model for sapphirine of Kelsey *et al*. (2004). The data files used in the calculations are given in Appendix S1. We begin with a discussion of the full system NCKFMASH to justify simplification to the FMAS(H) model system for subsequent calculations. Although biotite and rare feldspar are present in the rocks, components such as K, Ca and Na are not expected to play a significant role for this particular lithology. Biotite is mainly a retrograde phase and does not appear to have been involved in reactions in the segment of the *P*–*T* path that we are interested in modelling. Feldspar is extremely scarce, and is usually associated with cordierite. In terms of our treatment of H_2O, the system is further simplified by considering H_2O in terms of variable a_{H_2O}, instead of including melt as a phase, which is the likely source of H_2O in cordierite. The reasons for this will be discussed later. The first set of calculations considers the following phases: garnet, orthopyroxene, sillimanite, sapphirine and quartz. Subsequently, cordierite is added for the relevant domains involving the growth of this phase.

Pseudosections were first constructed for the bulk rock composition in order to estimate peak metamorphic conditions. Subsequent calculations assume that reaction is largely confined to discrete mineralogical domains with distinct domainal chemical compositions, as indicated by the microstructures. *P*–a_{H_2O} and

T–a_{H_2O} diagrams are used to explore the retrograde history of the rock in terms of the individual grain-boundary compositional domains described above. These individual domains are then used to explore the different reaction microstructures in order to look at the consistency of evolution in P–T between different compositional domains. It is assumed that a domainal analysis for the development of specific reaction microstructures should produce a self-consistent P–T evolution for it to be considered acceptable as a model for the P–T evolution of the rock. Bulk compositions were calculated using mineral proportions and mineral chemistry (Table 2).

Peak pressure–temperature conditions

In order to estimate peak metamorphic conditions, pseudosections in both the NCKFMASH and FMAS systems were calculated for the bulk composition corresponding to modal proportions of minerals inferred to have been the stable assemblage at peak P–T conditions (Fig. 6). The bulk composition was calculated by estimating modes of these phases (orthopyroxene 30%, garnet 20%, sillimanite 10%, quartz 40%) and using analysed mineral chemistry data (Tables 1 & 2). For the NCKFMASH calculations, small amounts of Na, Ca and K were added to this bulk composition to account for the trace modal amounts of biotite and feldspar in the samples at this locality.

Figure 6(a) is a P–T pseudosection calculated in NCKFMASH. The important difference between this diagram and Fig. 6(b), the FMAS pseudosection, is the presence of cordierite below about 7 kbar. Otherwise the topology of the diagrams is identical. Differences in the precise locations of the field boundaries are attributed to the incorporation of a small amount of Ca in the garnet used in the NCKFMASH bulk composition calculation. Because of the overall similarities in phase equilibria for these two bulk compositions, the system is simplified to FMAS(H) for further calculations and cordierite is only considered in the grain-boundary domains of interest.

It is instructive to compare Fig. 6(b) to published FMAS petrogenetic grids (e.g. Hensen, 1986; Powell & Sandiford, 1987; Hensen & Harley, 1990; Bertrand *et al.*, 1991; Audibert *et al.*, 1995; Carrington & Harley, 1995a,b; Harley, 1998a). An important feature of Fig. 6 is that the spinel-absent FMAS univariant reaction (2) mentioned earlier occurs within this particular bulk composition. Reaction (2) has a steep slope separating the divariant fields garnet–orthopyroxene–sillimanite–quartz and garnet–sapphirine–orthopyroxene–quartz, both of which are diagnostic of UHT metamorphic conditions.

Across reaction (2), orthopyroxene is destabilized in this bulk composition. Garnet becomes progressively more Fe-rich with decreasing P–T (Fig. 6b). Orthopyroxene X_{Mg} contours are slightly steeper than the garnet contours and also show a decrease in X_{Mg} with pressure decrease with slightly decreasing X_{Mg} with T decrease. Alumina content in orthopyroxene is strongly temperature-dependent, with steep y_{Opx} contours (Hensen & Harley, 1990). The y_{Opx} values within the garnet–orthopyroxene–sillimanite–quartz divariant field range from 0.18 to 0.24 at 900–1050 °C. Within the garnet–sapphirine–orthopyroxene–quartz divariant field, the contours are more widely spaced and y_{Opx} values range from 0.25 to 0.27 at 1050–1130 °C.

Based on the petrographic analysis above, the peak assemblage at UHT conditions is interpreted as garnet–orthopyroxene–sillimanite–quartz. The mineral proportion and compositions in ML-67 show that this divariant assemblage in FMAS occurs over a broad temperature range at 7–10 kbar, but mineral composition contours constrain the peak P–T conditions to approximately 960–1030 °C and 8–9 kbar (Fig. 6). For the purposes of constructing subsequent pseudosections, the peak conditions are taken to be represented by 8.75 kbar and 1025 °C, which lie within the P–T range based on the measured mineral compositions of the individual phases ($X_{Mg(Opx)} = 0.71$; $y_{Opx} = 0.23$; $X_{Mg(Grt)} = 0.61$).

Pressure–temperature path constraints

Following peak metamorphic conditions, the microstructural evolution of the rock is interpreted to develop domainally, based on the varied reaction microstructures preserved in the rock. Each of these reaction microstructures may be indicative of a different point or segment along the retrograde P–T path of the rock (e.g. Hensen, 1971; Harley, 1998b). In order to understand the mineral assemblage evolution

Table 2. Bulk compositions used in pseudosection analysis.

	Bulk rock	Domain 1: Grt–Sil	Domain 2: Grt–Qtz	Domain 3: Opx–Qtz
Mineral proportion	0.4 Qtz, 0.3 Opx, 0.2 Grt, 0.1 Sil	Grt:Sil (1:2) 0.33 Grt, 0.67 Sil	0.83 Qtz, 0.15 Grt, 0.02 Sil	0.83 Qtz, 0.15 Opx, 0.02 Sil
Mineral chemistry	X_{Mg}(Grt) = 0.61 X_{Mg}(Opx) = 0.71 y_{Opx} = 0.23	X_{Mg}(Grt) = 0.60	X_{Mg}(Grt) = 0.61	X_{Mg}(Opx) = 0.72 y_{Opx} = 0.20
Molar % oxides				
SiO_2	67.66	47.62	90.60	91.27
Al_2O_3	9.69	38.10	2.98	1.62
MgO	15.23	8.57	3.92	5.12
FeO	7.43	5.71	2.51	1.99

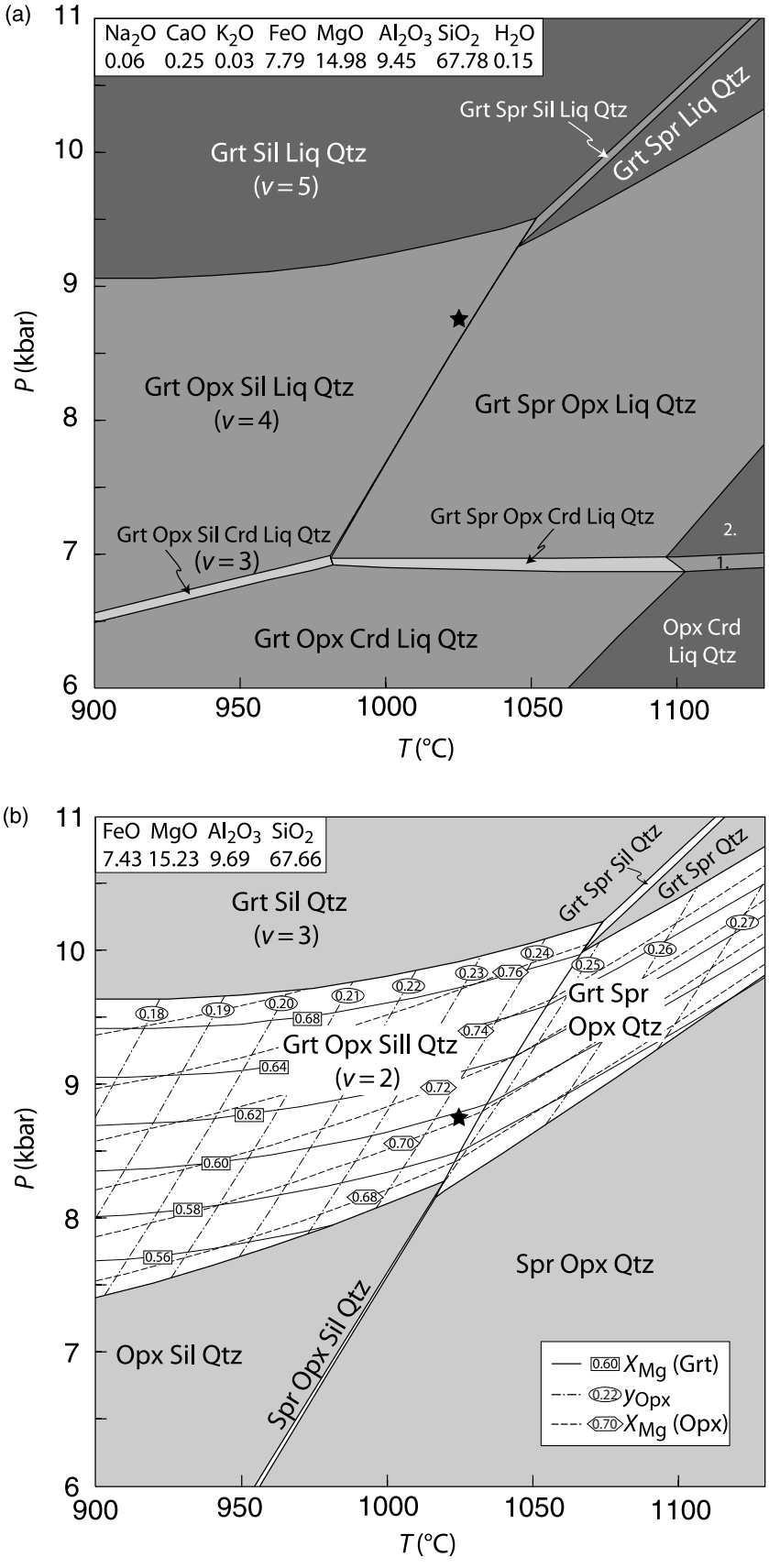

Fig. 6. (a) NCKFMASH *P–T* pseudosection for the bulk rock based on mineral proportions and mineral chemistry. 1. Spr Opx Crd Liq Qtz, 2. Spr Opx Liq Qtz. (b) *P–T* pseudosection for the bulk rock based on mineral proportions and mineral chemistry. Isopleths for mineral chemistry of garnet and orthopyroxene. Star indicates peak *P–T* conditions in the garnet–orthopyroxene–sillimanite–quartz divariant of 8.75 kbar, 1025 °C. Note that this estimation of peak *P–T* conditions is independent of the rock's bulk composition because this is within an FMAS divariant field. Decompression across the univariant reaction Opx + Sil = Grt + Spr + Qtz will stabilize the assemblage sapphirine–quartz.

and changing equilibration volume of these domains, the phase relationships are modelled at each grain boundary where a specific reaction microstructure develops. Calculated compatibility diagrams are used to show how equilibration volumes may change, as well as to predict how assemblages will develop along various points of the *P–T* path. Then pseudosections were constructed for specific domains using the grain-boundary compositions described above, in order to estimate *P–T* conditions for the development of specific reaction microstructures.

The reaction microstructure around sillimanite inclusions in garnet in domain 1 (garnet–sillimanite) provides a robust constraint on the general retrograde *P–T* evolution of this sample. Development of this reaction microstructure involves: (1) decompression across univariant reaction (2) with production of sapphirine–quartz; (2) evolution within the garnet–sillimanite–sapphirine–quartz divariant field (evolving via divariant equilibria 1); and (3) cooling and recrossing of reaction (2) involving the destabilization of sapphirine–quartz (Fig. 7). This evolution is simplified as a two segment *P–T* path (Fig. 7), involving isothermal decompression followed by isobaric cooling. A two segment *P–T* path will be used in subsequent diagrams, where the segments connect the following points: peak conditions at 8.75 kbar and 1025 °C, via isothermal decompression to 8.2 kbar and then via isobaric cooling to an arbitrary value of 980 °C.

Compatibility diagrams may be used to explore changes in mineral assemblage for a particular bulk composition or for the composition of individual domains during this evolution. The $FeO–MgO–Al_2O_3–SiO_2$ compatibility diagram, in which all compositions are considered to be quartz-saturated (Fig. 7), may be used to explore both the assemblage evolution and the changing equilibration volume of the garnet–sillimanite grain-boundary domain (domain 1). These compatibility diagrams are shown at three points along the *P–T* evolution: peak conditions; the knee of the segmented *P–T* path; and, a point along the cooling path (Fig. 7).

For calculation of a pseudosection for the garnet–sillimanite grain boundary, a domainal composition must be defined, noting that this composition is to represent an evolving range of compositions as shown in the compatibility diagrams in Fig. 7. For this purpose, garnet and sillimanite are combined in the proportions 2:1 (Table 2), using the core garnet composition. The resulting *P–T* pseudosection for this composition shows the main features of the microstructural evolution of this domain (Fig. 8). Along a decompression path at 1025 °C, the domain will develop sapphirine–quartz at around 8.4 kbar (Fig. 8). Because of the steepness of reaction (2), cooling results in recrossing of this reaction, leading to production of garnet and sillimanite at the newly formed sapphirine–quartz grain boundaries (Fig. 7). This *P–T* evolution implies that decompression is required to stabilize sapphirine–quartz. One problem with this pseudosection for the garnet–sillimanite grain boundary is that it predicts that new orthopyroxene will grow as reaction (2) is re-crossed, albeit in small amounts (Figs 8 & 9c). As discussed above with regard to the sequential evolution represented by the compatibility diagrams (Fig. 7), this artefact is a consequence of the composition used to draw the pseudosection, in a context where there is a range of compositions involved, and where the size of equilibrium domain and therefore the composition is evolving as *P–T* changes.

To represent domains that are SiO_2-undersaturated as well as quartz-bearing (Fig. 9), an $Al_2O_3–FeSiO_3–MgSiO_3$ (+ sillimanite) compatibility diagram is used. Triangles 1 and 3 highlight the possibility of different domains in a rock being quartz- and sapphirine-bearing, but sapphirine–quartz not being an equilibrium mineral assemblage. This is a common feature in granulites, reflecting the fact that SiO_2-undersaturated sapphirine-bearing mineral assemblages have a much wider *P–T* stability range than sapphirine–quartz. In the context of the garnet–sillimanite grain boundary analysis discussed above, initial decompression towards univariant reaction (2) sees a range of compositions representing the grain boundary located along the garnet–quartz edge of the garnet–orthopyroxene–quartz tie triangle, moving with it as pressure decreases. Across the univariant reaction, if the garnet is still in communication with the distal orthopyroxene as argued above, then the equilibria cannot be represented on these diagrams as they are calculated for sillimanite in excess. However, if garnet adjacent to sillimanite is not in communication with orthopyroxene, then triangle 2 on Fig. 9 shows that garnet–sapphirine–quartz–sillimanite forms a stable assemblage. This tie triangle moves first to the left then to the right as the rock follows the knee bend in the *P–T* path, involving the growth and then resorption of sapphirine and quartz. On recrossing the univariant reaction (2), the composition range at the grain boundary moves to the garnet–quartz edge of the garnet–orthopyroxene–quartz tie triangle or the garnet–sapphirine edge of the garnet–orthopyroxene–sapphirine tie triangle.

Cordierite and activity of H_2O

The approach of modelling domains within the rock allows an examination of the stability of cordierite and an evaluation of the importance of local variations in a_{H_2O} in controlling the presence or absence of cordierite along the retrograde path (see also Harley & Carrington, 2001; Thompson *et al.*, 2001; Harley *et al.*, 2002). The problem is approached by assuming that the source of H_2O that allows cordierite to grow is a melt phase, and that H_2O reaches the grain-boundary site via a chemical potential gradient. As there is no evidence as to what the composition of the melt might have been, the dimensions of the system are simplified by using a_{H_2O} as

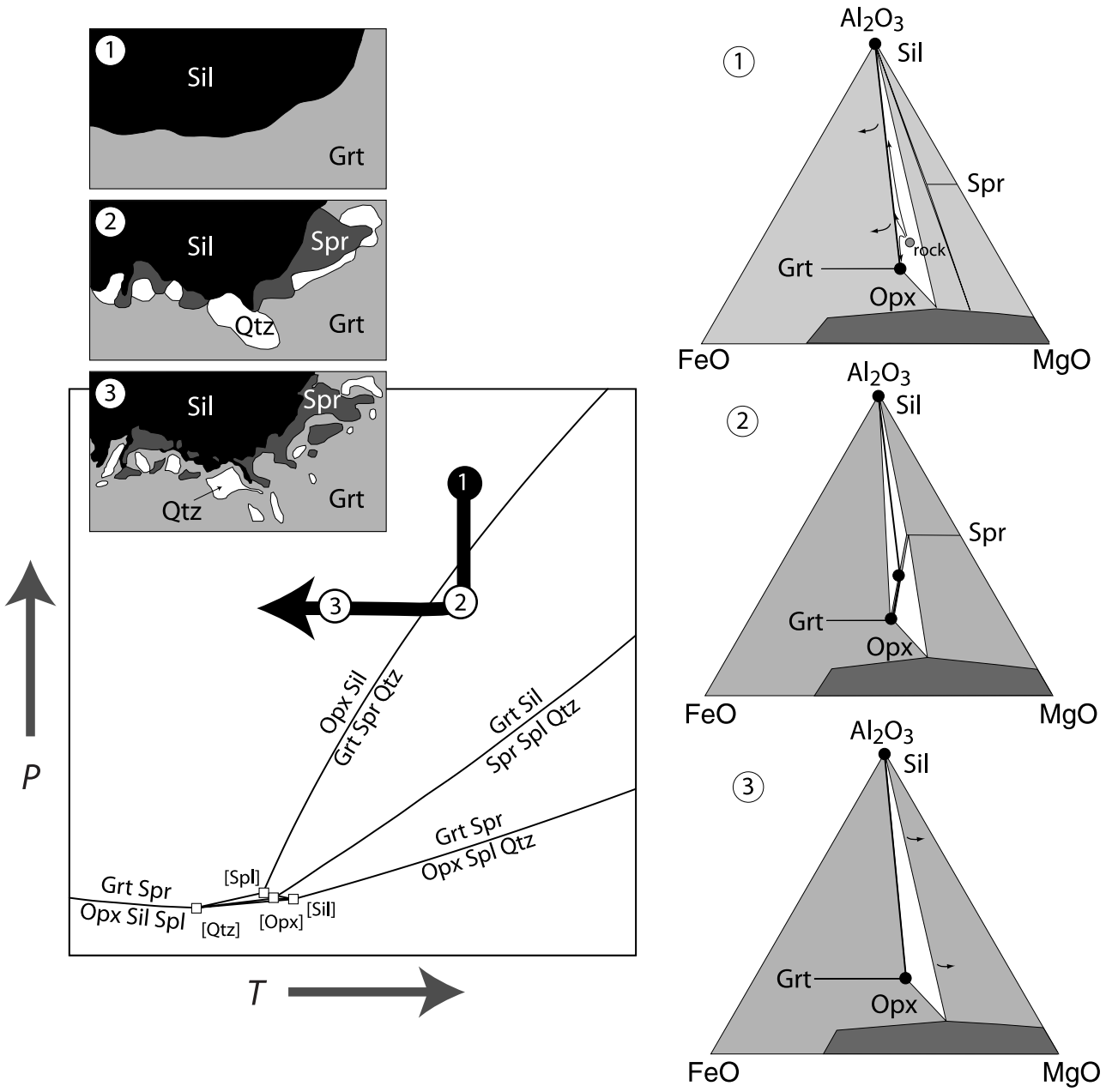

Fig. 7. *P–T* projection and sketches showing development of sapphirine–quartz around sillimanite inclusions in garnet. Calculated Al_2O_3–FeO–MgO compatibility triangles projected from quartz are shown at right for three points along the *P–T* path. Triangles are calculated for a dogleg *P–T* path representing a composite isothermal decompression isobaric cooling path from 8.75 kbar, 1025 °C to 8.2 kbar, 1025 °C to 8.2 kbar 980 °C. This path represents decompression and crossing of the univariant reaction Opx + Sil = Grt + Spr + Qtz, followed by recrossing of the reaction during cooling. Initially the rock resides in the garnet–orthopyroxene–sillimanite–quartz divariant field (grey circle in top compatibility diagram). At the start of decompression, the composition of the equilibration volume moves to, then lies along the garnet–sillimanite edge of the garnet–sillimanite–orthopyroxene triangle, as a range of compositions that are garnet-dominated within the garnet, and more sillimanite-rich within the sillimanite inclusion. On crossing the univariant reaction, the one remaining tie line between orthopyroxene and sillimanite is replaced by a tie line between garnet and sapphirine, and the range of domainal compositions remains on the garnet–sillimanite edge of the garnet–sillimanite–sapphirine triangle. On further decompression, the garnet–sapphirine–sillimanite and garnet–sapphirine–orthopyroxene triangles move further to the left. Progressively more of the lower part of the composition range may communicate with the distal orthopyroxene, and moves to the garnet–sapphirine edge of the garnet–sapphirine–orthopyroxene triangle. On cooling prior to recrossing the univariant reaction, the garnet–sapphirine–sillimanite triangle moves back causing the proportions of sapphirine (and quartz) to decrease, in favour of garnet and sillimanite. On recrossing the univariant reaction, the garnet–sapphirine tie line is no longer stable, and the garnet–orthopyroxene equilibrium once again operates to control the Fe–Mg equilibrium distribution and the composition of the equilibration volume again lies along the garnet–sillimanite edge of the garnet–sillimanite–orthopyroxene triangle.

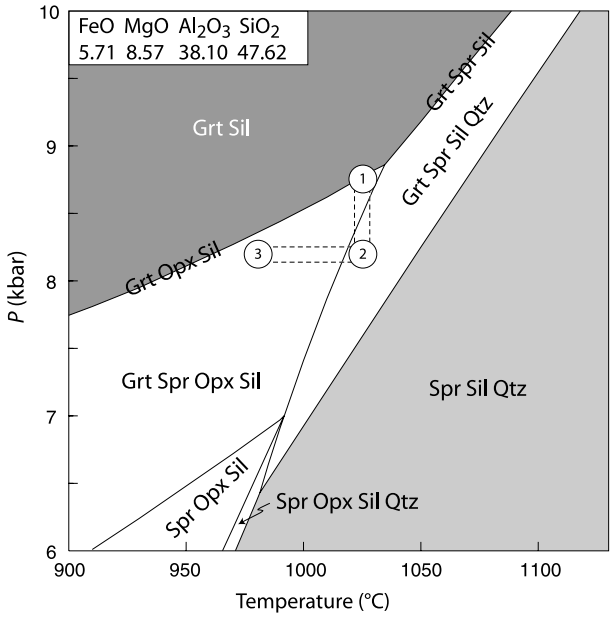

Fig. 8. *P–T* pseudosection for a domainal bulk composition representing the garnet–sillimanite grain boundary (see text). Numbers indicate *P–T* locations for compatibility triangles in (b). Decompression produces the stable sapphirine–quartz assemblage.

the controlling variable, thus allowing an examination of the role of H_2O within the FMASH system.

The range of a_{H_2O} involved and the estimation of *P–T* conditions of cordierite-producing reactions may be examined by construction of pseudosections using the domainal compositions for garnet–quartz (domain 2) and orthopyroxene–quartz (domain 3) grain-boundary domains. These diagrams demonstrate that cordierite may be produced along a *P–T* path consistent with the overall *P–T* path constrained by microstructures that do not involve cordierite (e.g. domain 1). Thus the presence or absence of cordierite may be explained by local variations of a_{H_2O} (e.g. lower a_{H_2O} within garnet than at its grain boundary).

This concept is illustrated through a series of compatibility diagrams, at fixed pressure and temperature, constructed for progressively increasing steps in a_{H_2O} from 0 to 0.4 (Fig. 10). This series of diagrams demonstrates that the H_2O content for different compositions varies, because with increasing a_{H_2O} the tie lines to cordierite are seen to include a broader range of compositional space. At 8.75 kbar and 1025 °C, cordierite first appears in the compatibility diagram at an a_{H_2O} of approximately 0.2 through the MAS reaction:

$$\text{Spr} + \text{Opx} = \text{Crd}. \quad (3)$$

With increasing a_{H_2O}, cordierite stability extends by the FMASH univariant reaction:

$$\text{Spr} + \text{Qtz} = \text{Opx} + \text{Crd} + \text{Sil}. \quad (4)$$

Finally, at sufficiently high a_{H_2O} values (>0.35), cordierite is further stabilized by the FMASH univariant reaction:

$$\text{Opx} + \text{Sil} + \text{Qtz} = \text{Grt} + \text{Crd}. \quad (5)$$

As a_{H_2O} increases, cordierite stability extends over a progressively wider range of bulk compositions (Fig. 10).

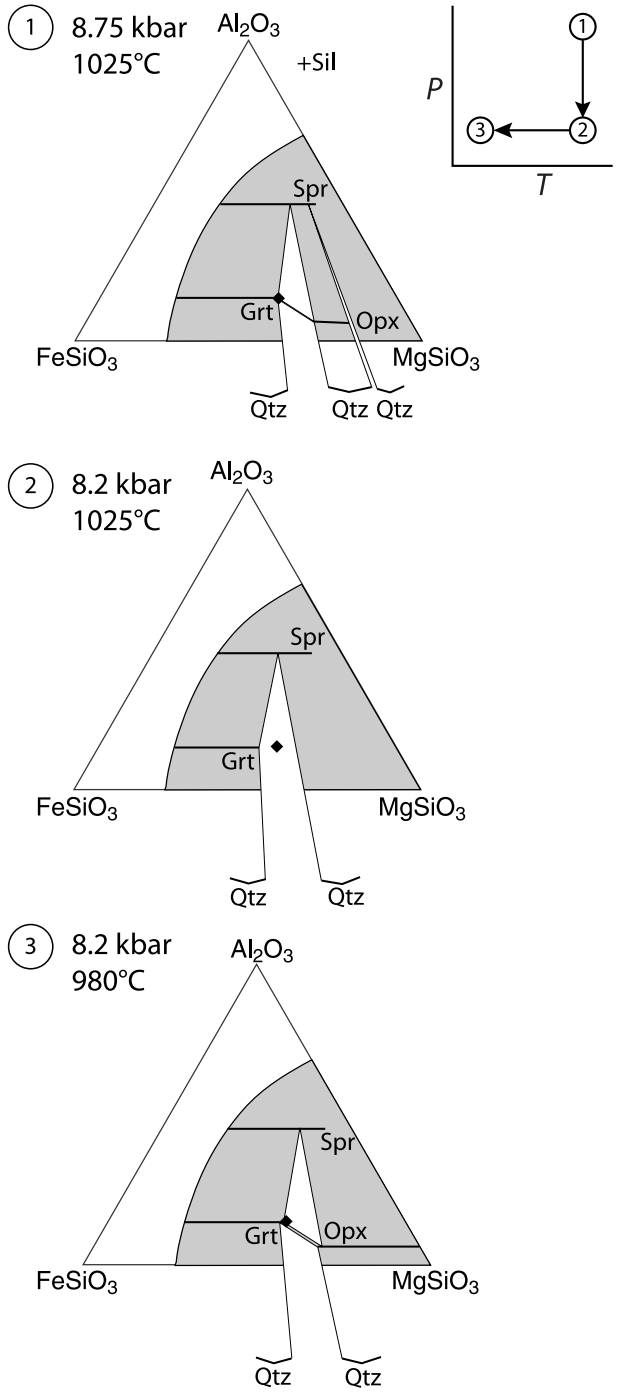

Fig. 9. Calculated Al_2O_3–$FeSiO_3$–$MgSiO_3$ compatibility triangles projected through sillimanite. Triangles are calculated for the dogleg *P–T* path shown in (a). See text for discussion.

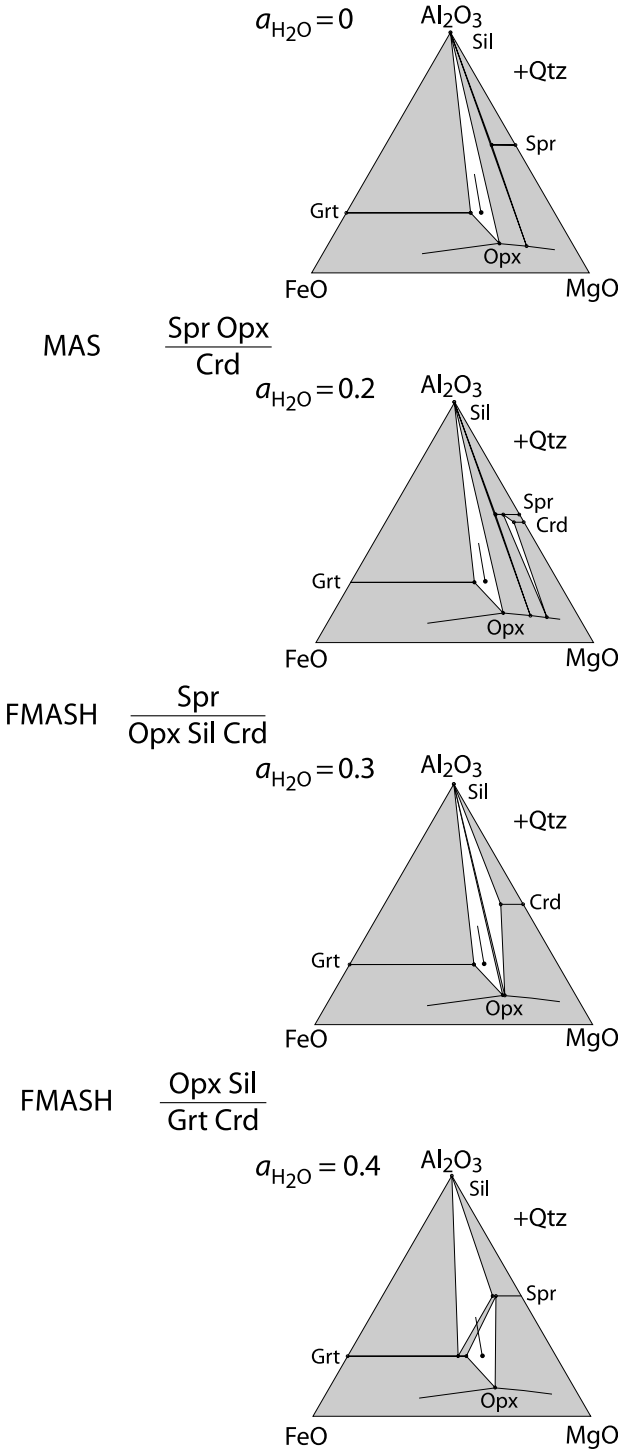

Fig. 10. Calculated Al_2O_3–FeO–MgO compatibility triangles projected from quartz for 8.75 kbar and 1025 °C showing the effect of varying a_{H_2O} on the stability of cordierite. Dot represents a garnet–quartz dominated bulk composition. Line emanating from dot represents a variation in sillimanite in the bulk. For a bulk composition that corresponds to the dot, the rock initially resides in the garnet–orthopyroxene–sillimanite–quartz divariant but with increasing a_{H_2O}, cordierite first stabilized by the addition of H_2O and with increasing a_{H_2O}, is produced by the reaction Opx + Sil + H_2O = Grt + Crd.

To envision what happens to a_{H_2O} during the evolution of the mineral assemblage, we start by assuming that the initial a_{H_2O} is at some arbitrary low value. An increase in a_{H_2O} occurs when a chemical potential gradient in H_2O is established through the local proximity of melt. When that happens, if cordierite is stabilized, cordierite grows and the water content of the rock increases. Assuming that there is just one such increase in a_{H_2O} due to influx of melt, the assemblage will continue to evolve at constant H_2O content, which approximately equals the cordierite mol.%. This concept is illustrated schematically in Fig. 11, which is a *P–T* path *v.* a_{H_2O} projection. This diagram displays the isothermal decompression and isobaric cooling segments on a composite *P–T v.* a_{H_2O} diagram, with isothermal decompression at 1025 °C, followed by isobaric cooling at 8.2 kbar.

As cordierite is present only in the reaction microstructures, the a_{H_2O} must have been lower than that required to stabilize cordierite before any reaction. The point along the *P–T* path where this spike in a_{H_2O} (corresponding to the minimum a_{H_2O} value that would result in cordierite growth) may be evaluated by studying the reaction microstructures preserved in the grain-boundary domains. For example, sillimanite has replaced sapphirine at the garnet–quartz grain boundary prior to cordierite growth. This implies that sapphirine was produced following the peak conditions (Fig. 3k), and subsequently this was replaced by sillimanite. Figure 11 shows that in order for this microstructure to occur, the mineral assemblage would first cross univariant reaction (2), entering the sapphirine stability field in the knee of the two-segment decom-

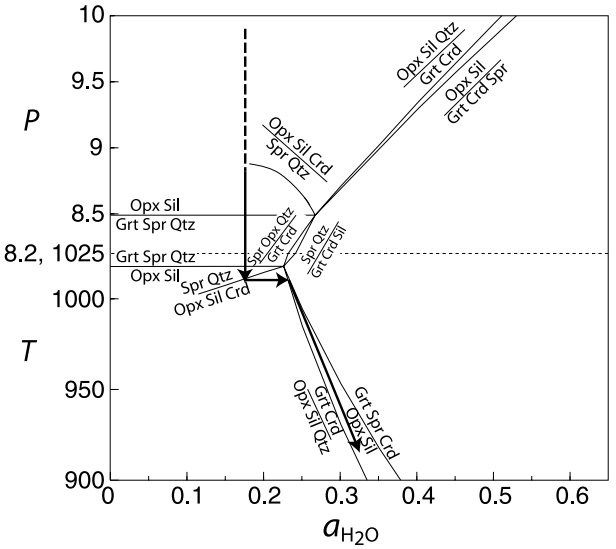

Fig. 11. Schematic illustrating *P–T* path *v.* a_{H_2O} path. Isothermal decompression from 10 to 8.2 kbar at 1025 °C followed by isobaric cooling at 8.2 kbar. Dogleg *P–T* path. Crossing and recrossing of FMAS univariant Opx + Sil = Grt + Spr + Qtz reaction.

pression-cooling P–T path. Further cooling would result in growth of new sillimanite at the expense of sapphirine as reaction (2) is recrossed. Only then does the grain boundary experience the a_{H_2O} spike and cordierite grows, as shown schematically by the horizontal part of the arrowed path on Fig. 11.

Reactions represented by these microstructural relationships may be examined in pseudosections constructed for compositions of grain-boundary domains, allowing analysis of the resulting stable mineral assemblages (Fig. 12). The compositions for both the garnet–quartz and orthopyroxene–quartz domains were calculated with the mineral compositions of garnet and orthopyroxene, by combining garnet (or orthopyroxene), quartz, and sillimanite in the proportions 15% garnet (or orthopyroxene), 83% quartz and 2% sillimanite (Table 2). This effectively emulates the grain boundary because in both domains the large porphyroblasts typically have small, euhedral sillimanite grains at their rims, and the porphyroblasts are completely surrounded by quartz (Figs 4d,e & 5). For both of these domains all mineral assemblages are assumed to be quartz-saturated, and this is reflected in the compositions chosen.

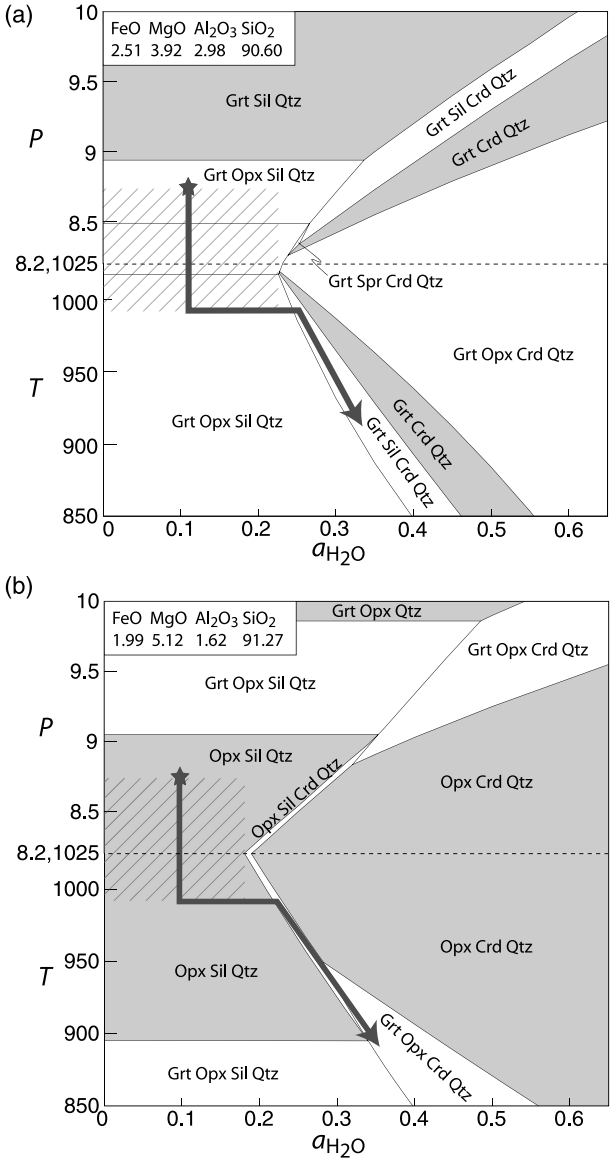

Fig. 12. P–T path *v.* a_{H_2O} pseudosections. P–T path is isothermal decompression (10–8.2 kbar, 1025 °C) followed by isobaric cooling (1025–900 °C, 8.2 kbar). Thick grey line marks one possible P–T–a_{H_2O} path showing the incoming of cordierite. Shaded field marks possible range of values of a_{H_2O}.
(a) Orthopyroxene–quartz grain-boundary composition,
(b) garnet–quartz grain-boundary composition.

Figure 12 shows a pseudosection of P–T path *v.* a_{H_2O} for the garnet–quartz (domain 2) and orthopyroxene–quartz (domain 3) grain-boundary domains. Figure 12(a) is the pseudosection for the specific sapphirine–sillimanite microstructure discussed above. This diagram implies that the temperature at which a_{H_2O} was increased was likely to be < 1015 °C with a minimum a_{H_2O} value of about 0.23. The a_{H_2O} value prior to the introduction of cordierite into the assemblage could have been any value < 0.23. Following the introduction of cordierite, the domain would evolve along an isopleth of constant H_2O content, corresponding approximately to a constant cordierite mol.%, shown by the arrow through the cordierite stability field in Fig. 12(a). Figure 12(b) shows a similar evolution for the orthopyroxene–quartz grain boundary (domain 3). Cordierite and eventually garnet are expected to be produced along the P–T–a_{H_2O} path for this domain (Fig. 12b).

DISCUSSION

Pressure–temperature evolution of the Anápolis–Itauçu Complex

Modelling of mineral equilibria of Mg–Al-rich UHT granulites at a locality in the AIC, central Brazil, indicates that formation of the early, coarse-grained mineral assemblage of garnet–orthopyroxene–sillimanite–quartz occurred at about 9 kbar and 1000 °C. Mineral assemblages and reaction microstructures, combined with phase modelling, suggest a two-stage retrograde P–T path. First, sapphirine–quartz developed during decompression across the Opx + Sil = Grt + Spr + Qtz FMAS univariant reaction. Whether there was any increase in temperature associated with this decompression cannot be evaluated in our analysis. Second, sapphirine–quartz was destabilized by isobaric cooling that led to recrossing of the univariant reaction. The growth of cordierite occurred across the Opx + Sil + Qtz = Grt + Crd FMASH univariant reaction in certain grain-boundary compositional domains. Thus, a P–T path consistent with the observed microstructures involves a component of decompression (< 1 kbar) followed by cooling (< 100 °C).

We use local variation in a_{H_2O} to explain the growth of cordierite, which need not imply significant decompression from peak *P–T* conditions, which is traditionally inferred from the presence or absence of cordierite in UHT granulites based on the limits inferred from traditional petrogenetic grids (e.g. Harley *et al*., 1990; Ouzegane & Boumaza, 1996; Sajeev & Osanai, 2004; Sajeev *et al*., 2004). In addition, it is possible that variation in a_{CO_2} is also involved, given the analysed CO_2 content of the ML67 cordierite. However, concerns with open-system behaviour of H_2O and CO_2 in natural cordierite (Harley *et al*., 2002) make analyses of cordierite for H_2O and CO_2 difficult to use: the H_2O and CO_2 contents of cordierite may not reflect conditions when the cordierite grew. Regardless, even if CO_2 is involved, the inferred evolution will be little affected. If CO_2 is significant in the development of cordierite, then in Fig. 11 the *x* axis can be thought of as a cypher for the action of both a_{CO_2} and a_{H_2O}.

Moraes *et al*. (2002) interpreted minimum *P–T* conditions at the metamorphic peak as 1030–1050 °C at around 10 kbar, but suggest that Al_2O_3 contents in orthopyroxene may indicate temperatures that possibly exceeded 1150 °C. Additionally, Moraes *et al*. (2002) inferred a clockwise *P–T* path and speculated that the maximum pressure was likely to have been substantially greater than 10 kbar and pre-dated the attainment of maximum temperature. Based on mineral chemistry, our results suggest that maximum temperatures were not as extreme as 1150 °C and that pressures at maximum temperatures were < 10 kbar. The interpretations of Moraes *et al*. (2002) were derived using the FMAS petrogenetic grid of Harley (1998a), which, as discussed previously, is inferred by Kelsey *et al*. (2004) to represent an essentially constant a_{H_2O} grid. The interpretations based on the Harley (1998a) approach assume that [Spl] is an FMAS invariant in FMAS at 10.2 kbar, 1050 °C, whereas in fact [Spl] is an FMASH univariant line as discussed earlier. According to Kelsey *et al*. (2004), the actual FMAS invariant point is at 6.7 kbar, 990 °C (Fig. 1). Harley's [Spl] is just a position on this FMASH line, corresponding to an a_{H_2O} (0.45) that is much higher than that deduced for the cordierite-bearing domains in these rocks (Fig. 11).

Moraes *et al*. (2002) interpret the *P–T* path to involve decompression along a path approximately parallel to an isopleth of constant Al_2O_3 in orthopyroxene. Based on the absence of cordierite in their sample suite from this locality, Moraes *et al*. (2002) concluded that the rock stayed at pressures greater than the garnet–orthopyroxene–sillimanite–quartz divariant down to 900 °C, and never entered the cordierite stability field. Based on microstructural relationships and the calculated equilibria, sapphirine–quartz is inferred as forming along the initial decompression path. In this suite of samples, we observe small amounts of cordierite in some samples from this locality. As shown in the domain pseudosection modelling, the formation of cordierite is consistent with the *P–T* path constrained from modelling the development of the sapphirine–quartz microstructure after garnet–sillimanite. This modelling suggests that the presence or absence of cordierite need not imply a particular maximum pressure (e.g. around 10 kbar), as is generally inferred.

The suite of samples investigated in this study contains both cordierite-present and cordierite-absent rocks, that have evolved along the same *P–T* path. In order to accurately assess the *P–T* evolution each rock sample, and in fact each individual domain within the rock, must be handled as different chemical compositions. Arguably, the most sensitive compositional constraint is a_{H_2O}, as the position of the 'FMAS' invariant points is strongly affected by this variable. It is inferred that these samples evolved along a clockwise *P–T* path, but at conditions that were not as extreme as previously inferred and where the decompression segment may be more limited than inferred by Moraes *et al*. (2002).

This type of approach should be used to document distribution of temperatures across the entire AIC, as other 'common' granulites may record a similar history. It may simply be that only rocks of particular Mg–Al-rich compositions record the diagnostic UHT mineral assemblages (Kelsey *et al*., 2003). Alternatively, there may be localized heating in the vicinity of the UHT localities that have been identified. In addition, the recognition of the importance of a_{H_2O} for the FMASH [Spl] equilibrium implies that many UHT granulites may evolve at lower pressures than was previously thought, and thus at lower crustal conditions that do not require an extreme overthickened crust. Through application of quantitative pseudosections across the AIC, it should be possible to constrain the regional extent of UHT metamorphism and allow for a more thorough assessment of the regional tectonic evolution of the area in terms of models that advocate widespread *v*. localized heating.

Pitfalls with traditional thermobarometric techniques

Grids for metapelite compositions

Petrogenetic grids involving mineral equilibria in the FMAS and KFMASH systems have traditionally been used for analysis of the changes in pressure and/or temperature implied by reaction microstructures in aluminous granulites (Hensen & Green, 1973; Bertrand *et al*., 1991; Carrington & Harley, 1995a,b; Harley, 1998a). However, such experimentally derived grids allow only qualitative interpretations, and, as has been addressed earlier, have significant uncertainty with respect to hydrous phases. The position of the invariant points in FMAS is a function of a_{H_2O}, many

assemblages evolve via multivariant rather than univariant equilibria, and most of these rocks exhibit pervasive arrested reaction microstructures implying equilibration on short length-scales. Absolute *P–T* paths derived from such grids are subject to large, inherent uncertainties. It is important to recognize that the FMASH calculations used in this study are only applicable to low-Fe^{3+} assemblages. The stability of spinel in quartz-bearing assemblages is restricted in the low f_{O_2} grid of Hensen (1986), but is expanded at high f_{O_2} conditions (Hensen, 1986; Powell & Sandiford, 1987).

Aluminium solubility in orthopyroxene thermometry

It is generally accepted that Fe–Mg exchange thermometry in granulites commonly yields lower temperatures than the metamorphic peak because of compositional re-equilibration of minerals during cooling (Frost & Chacko, 1989). This has led to the use of retrieval calculations that involve the back calculation of the Fe–Mg compositions of the participating phases until the pressure estimate overlaps with the reference pressure for that sample (Fitzsimons & Harley, 1994; Pattison & Begin, 1994; Pattison *et al.*, 2003), if such a reference pressure is available. Application of these techniques has confirmed that high content of Al_2O_3 in orthopyroxene (8–13 wt%) is one of the most reliable indicators of UHT conditions (Harley, 1989, 1998a). However, estimating peak temperature conditions using aluminium solubility in orthopyroxene has large uncertainties because of discrepancies in contour positioning that depend on the data sets and experiments that are used.

Thermometry using aluminium solubility in orthopyroxene may be useful in constraining the *P–T* paths of UHT granulites when zoning in orthopyroxene is present. For example, Harley & Motoyoshi (2000) observed two generations of orthopyroxene in UHT granulites from Enderby Land, Antarctica that equilibrated at different temperatures, which implies at least a 60–80 °C difference in temperature. This type of relative thermometry is useful; however, the actual peak temperatures implied by the maximum Al_2O_3 contents of 12.2 wt% ($y_{Opx} = 0.245$) are subject to debate depending on the calibration chosen. The Harley & Motoyoshi (2000) calibration yields temperatures well in excess of 1120 °C whereas our calculations using the thermodynamic database of Holland & Powell (1998) yield temperatures of around 1000–1060 °C. Likewise, Moraes *et al.* (2002) inferred that temperatures in the AIC may have exceeded 1150 °C based on the Harley & Motoyoshi (2000) calibration. However, the results from this study suggest that the Al content of orthopyroxene places a maximum temperature constraint of around 1030 °C. The reasons for this discrepancy are beyond the scope of this study, but warrant further examination.

Implications for *P–T* paths of UHT granulites

This study highlights a new quantitative approach to interpreting the metamorphic evolution of UHT granulites by constructing pseudosections for specific local bulk compositions, which builds upon previous approaches that applied qualitative and semi-quantitative methods to assess the evolution of reaction microstructures (coronae, symplectites) along the *P–T* path. As a consequence of this approach, there are some implications for the *P–T* paths of other occurrences of UHT granulites. Each case must be handled separately for the observed reaction microstructural relationships, using appropriate compositions for the domains involved. One pitfall in the application of conventional techniques may be illustrated by a consideration of the isothermal decompression *P–T* paths that have been proposed for a number of UHT terranes. Commonly, the *P–T* paths are based on a transition from orthopyroxene–sillimanite–quartz or sapphirine–quartz to garnet–cordierite-bearing assemblages (e.g. Harley *et al.*, 1990). We briefly consider three representative decompression *P–T* paths proposed for UHT granulites – from southern India, Sri Lanka, and the In Ouzzal granulite unit, Algeria (Ouzegane & Boumaza, 1996; Sajeev *et al.*, 2004; Sajeev & Osanai, 2004). In this discussion, the conclusions of the authors are compared with a reappraisal based on the methodology used above, accepting that such a comparison is in danger of being superficial without access to the rocks and considering specifically the domainal equilibria involved in each case. For the purposes of this comparison, the peak metamorphic mineral assemblage proposed by the author are accepted, although it is possible in several of these studies that quartz is in domains that are separated from the other main diagnostic minerals, a potential problem that was alluded to above.

For the Madurai block of southern India, Sajeev *et al.* (2004) estimated peak conditions of 1000 ± 50 °C and 11 kbar, using garnet–orthopyroxene–plagioclase–quartz thermobarometry. Based on the mineral chemistry of the peak assemblage, we infer, in contrast, *P–T* conditions of 990–970 °C and 8.8–9.4 kbar. For the Central Highland Complex, Sri Lanka, Sajeev & Osanai (2004) estimated peak conditions based on similar methods to Sajeev *et al.*, 2004, yielding > 1100 °C and 12 kbar with sapphirine–quartz stable at the peak. The *P–T* evolution is constrained by zoning of Al in orthopyroxene using the calibration of Harley & Motoyoshi (2000). Based on the mineral chemistry of the peak assemblage, we infer *P–T* conditions of about 1110–1070 °C and 9.3 kbar. For In Ouzzal, Algeria, Ouzegane & Boumaza (1996) inferred peak *P–T* conditions of 1150 °C and 10 kbar, based on the stability of sapphirine–quartz using conventional FMAS grids. Again, based on the mineral chemistry of the peak assemblage, we infer *P–T* conditions of 1030–1000 °C and 9–10 kbar. This

reappraisal suggests lower temperatures and pressures, although errors on both values are likely to be several tens of degrees and 1–2 kbar.

Perhaps more important than the authors' elevated *P–T* estimates, is the large amount of decompression that was inferred in each of these studies, on the order of about 4 kbar, estimated on the basis of the development of cordierite and, during further cooling, retrograde biotite (e.g. Harley *et al*., 1990; Sajeev *et al*., 2004; Sajeev & Osanai, 2004). *P–T* conditions for the development of cordierite are generally based on Harley (1998a), but as has been shown in this study, the position of cordierite-forming (and biotite-forming) reactions are strongly dependent on a_{H_2O}. If a_{H_2O} is sufficiently low, cordierite-free peak metamorphic mineral assemblages will be stable at significantly lower pressures and, to a lesser extent, lower temperatures. The formation of cordierite then occurs at a slightly lower pressure than the cordierite-free peak, and the presence of cordierite only requires a small amount of decompression. Therefore, we suggest that the application of the approach outlined in this study will produce a better estimate of peak metamorphic conditions, and place better constraints on the retrograde *P–T* path.

CONCLUSIONS

The samples investigated in this study provide an ideal opportunity to model the metamorphic evolution of UHT granulite reaction microstructures because of the relatively simple mineralogy of the impure quartzites at this locality in the AIC. This approach allows for comparison with published petrogenetic grids. The AIC example provides evidence that small changes in pressure and temperature may produce a complex variety of microstructures and that temperatures of UHT metamorphism, although high, may not be as extreme as previously thought. In addition, local variations in a_{H_2O} are important in controlling the development of cordierite. The main advantages of the methods used in this study are: (1) the modelling approach is linked to composition, allowing an investigation of microscale equilibrium domains within a rock; and (2) the investigation of the importance of H_2O in the stability of cordierite is not possible using experimentally derived grids.

The approach we have followed has important implications for both conventional thermobarometric techniques and *P–T* projections that are generally applied in the interpretation of the metamorphic evolution of UHT granulites. The approach of understanding the evolution of multivariant assemblages, coupled with the ability to examine the effects of a_{H_2O}, provides important new opportunities for evaluating conditions of UHT metamorphism.

ACKNOWLEDGEMENTS

This work was supported by NSF grant EAR-0227553 to M.B., ARC grant DP0451770 to R.P., and CNPq grant 690078/02-1 to R.A.J. Trouw. We thank R. White for valuable discussions, I. Araújo and J. Villar for field assistance, P. Piccoli for assistance with microprobe analysis, and S. Harley for the ion probe measurements of cordierite and sapphirine at the University of Edinburgh. Constructive and thorough reviews by S. Harley, E. Essene, and an anonymous reviewer greatly improved the original manuscript.

SUPPLEMENTARY MATERIAL

The authors have provided the following supplementary material.

Appendix S1. NCKFMASH and FMAS THERMOCALC data files used in calculations.

REFERENCES

Audibert, N., Hensen, B. J. & Bertrand, P., 1995. Experimental study of phase relations involving osumilite in the system K_2O–FeO–MgO–Al_2O_3–SiO_2–H_2O at high pressure and temperature. *Journal of Metamorphic Geology*, **13,** 331–344.

Bertrand, P., Ellis, D. J. & Green, D. H., 1991. The stability of sapphirine–quartz and hypersthene–sillimanite–quartz assemblages: an experimental investigation in the system FeO–MgO–Al_2O_3–SiO_2 under H_2O and CO_2 conditions. *Contributions to Mineralogy and Petrology*, **108,** 55–71.

Boger, S. D. & White, R. W., 2003. The metamorphic evolution of metapelitic granulites from Radok Lake, northern Prince Charles Mountains, east Antarctica; evidence for an anticlockwise *P–T* path. *Journal of Metamorphic Geology*, **21,** 285–298.

Bohlen, S. R., 1987. Pressure–temperature–time paths and a tectonic model for the evolution of granulites. *Journal of Geology*, **95,** 617–632.

Bohlen, S. R., 1991. On the formation of granulites. *Journal of Metamorphic Geology*, **9,** 223–229.

Brown, M., 2002. Retrograde processes in migmatites and granulites revisited. *Journal of Metamorphic Geology*, **20,** 25–40.

Brown, M. & Raith, M., 1996. First evidence of ultrahigh-temperature decompression from the granulite province of southern India. *Journal of the Geological Society*, **153,** 819–822.

Carrington, D. P. & Harley, S. L., 1995a. Partial melting and phase relations in high-grade metapelites: an experimental petrogenetic grid in the KFMASH system. *Contributions to Mineralogy and Petrology*, **120,** 270–291.

Carrington, D. P. & Harley, S. L., 1995b. The stability of osumilite in metapelitic granulites. *Journal of Metamorphic Geology*, **13,** 613–625.

Fitzsimons, I. C. W. & Harley, S. L., 1994. The influence of retrograde cation exchange on granulite *P–T* estimates and a convergence technique for the recovery of peak metamorphic conditions. *Journal of Petrology*, **35,** 543–576.

Frost, B. R. & Chacko, T., 1989. The granulite uncertainty principle: limitations on thermobarometry in granulites. *Journal of Geology*, **97,** 435–450.

Guiraud, M., Powell, R. & Rebay, G., 2001. H_2O in metamorphism and unexpected behaviour in the preservation of metamorphic mineral assemblages. *Journal of Metamorphic Geology*, **19,** 445–454.

Harley, S. L., 1985. Garnet-orthopyroxene bearing granulites from Enderby Land, Antarctica: metamorphic pressure–temperature–time evolution of the Archean Napier Complex. *Journal of Petrology*, **26,** 819–856.

Harley, S. L., 1989. The origins of granulites: a metamorphic perspective. *Geological Magazine*, **126,** 215–247.

Harley, S. L., 1998a. On the occurrence and characterization of ultrahigh-temperature crustal metamorphism. In: *What Drives Metamorphism and Metamorphic Reactions?* (eds Treloar, P. & O'Brien, P.), Vol. 138, pp. 81–107. Geological Society Special Publications, London.

Harley, S.L., 1998b. Ultrahigh temperature granulite metamorphism (1050 °C, 12 kbar) and decompression in garnet (Mg70)–orthopyroxene–sillimanite gneisses from the Rauer Group, East Antarctica. *Journal of Metamorphic Geology*, **16,** 541–562.

Harley, S. L. & Carrington, D. P., 2001. The distribution of H_2O between cordierite and granitic melt: H_2O incorporation in cordierite and its application to high-grade metamorphism and crustal anatexis. *Journal of Petrology*, **42,** 1595–1620.

Harley, S. L. & Hensen, B. J., 1990. Archaean and Proterozoic high-grade terranes of East Antarctica (40–80 °E): a case study of diversity in granulite facies metamorphism. In: *High-temperature Metamorphism and Crustal Anatexis* (eds Ashworth, J. & Brown, M.), pp. 320–370. Unwin Hyman, London.

Harley, S. L. & Motoyoshi, Y., 2000. Al zoning in orthopyroxene in a sapphirine quartzite: evidence for >1120 °C UHT metamorphism in the Napier Complex, Antarctica, and implications for entropy of sapphirine. *Contributions to Mineralogy and Petrology*, **138,** 293–307.

Harley, S. L., Hensen, B. J. & Sheraton, J. W., 1990. Two-stage decompression in orthopyroxene-sillimanite granulites from Forefinger Point, Enderby Land, Antarctica; implications for the evolution of the Archaean Napier Complex. *Journal of Metamorphic Geology*, **8,** 591–613.

Harley, S. L., Thompson, P., Hensen, B. J. & Buick, I. S., 2002. Cordierite as a sensor of fluid conditions in high-grade metamorphism and crustal anatexis. *Journal of Metamorphic Geology*, **20,** 71–86.

Hensen, B. J., 1971. Theoretical phase relations involving cordierite and garnet in the system $MgO–FeO–Al_2O_3–SiO_2$. *Contributions to Mineralogy and Petrology*, **33,** 191–214.

Hensen, B. J., 1986. Theoretical phase relations involving cordierite and garnet revisited: the influence of oxygen fugacity on the stability of sapphirine and spinel in the system Mg–Fe–Al–Si–O. *Contributions to Mineralogy and Petrology*, **92,** 362–367.

Hensen, B. J. & Green, D. H., 1973. Experimental study of the stability of cordierite and garnet in pelitic compositions at high pressures and temperatures. III. Synthesis of experimental data and geological applications. *Contributions to Mineralogy and Petrology*, **38,** 151–166.

Hensen, B. J. & Harley, S. L., 1990. Graphical analysis of *P–T–X* relations in granulite facies metapelites. In: *High Temperature Metamorphism and Crustal Anatexis* (eds Ashworth, J. & Brown, M.), pp. 427–457. Unwin Hyman, London.

Holland, T. J. B. & Powell, R., 1998. An internally-consistent thermodynamic data set for phases of petrological interest. *Journal of Metamorphic Geology*, **16,** 309–343.

Hollis, J. A. & Harley, S. L., 2003. Alumina solubility in orthopyroxene coexisting with sapphirine and quartz. *Contributions to Mineralogy and Petrology*, **144,** 473–483.

Johnson, T. & Brown, M., 2004. Quantitative constraints on metamorphism in the Variscides of Southern Brittany – a complementary pseudosection approach. *Journal of Petrology*, **45,** 1237–1259.

Johnson, T., Brown, M. & Solar, G. S., 2003a. Low-pressure subsolidus and suprasolidus phase equilibria in the MnNCKFMASH system: constraints on conditions of regional metamorphism in western Maine, northern Appalachians. *American Mineralogist*, **88,** 624–638.

Johnson, T., Gibson, R. L., Brown, M., Buick, I. S. & Cartwright, I., 2003b. Partial melting of metapelitic rocks beneath the Bushveld Complex, South Africa. *Journal of Petrology*, **44,** 789–813.

Kelsey, D. E., White, R. W. & Powell, R., 2003. Orthopyroxene-sillimanite-quartz assemblages: distribution, petrology, quantitative *P–T–X* constraints and *P–T* paths. *Journal of Metamorphic Geology*, **21,** 439–453.

Kelsey, D. E., White, R. W., Holland, T. J. B. & Powell, R., 2004. Calculated phase equilibria in $K_2O–FeO–MgO–Al_2O_3–SiO_2–H_2O$ for sapphirine–quartz-bearing mineral assemblages. *Journal of Metamorphic Geology*, **22,** 559–578.

Kretz, R., 1983. Symbols for rock-forming minerals. *American Mineralogist*, **68,** 277–279.

McDade, P. & Harley, S. L., 2001. A petrogenetic grid for aluminous granulite facies metapelites in the KFMASH system. *Journal of Metamorphic Geology*, **19,** 45–59.

Moraes, R., Brown, M., Fuck, R. A., Camargo, M. A. & Lima, T. M., 2002. Characterization and *P–T* evolution of melt-bearing ultrahigh-temperature granulites: an examples from the Anápolis–Itauçu Complex of the Brasília fold belt, Brazil. *Journal of Petrology*, **43,** 1673–1705.

Ouzegane, K. & Boumaza, S., 1996. An example of ultrahigh-temperature metamorphism: orthopyroxene–sillimanite–garnet, sapphirine–quartz, and spinel–quartz parageneses in Al–Mg granulites from In Hihaou, In Ouzzal, Hoggar. *Journal of Metamorphic Geology*, **14,** 693–708.

Ouzegane, K., Guiraud, M. & Kienast, J. R., 2003. Prograde and retrograde evolution in high-temperature corundum granulites (FMAS and KFMASH systems) from In Ouzzal terrane (NW Hoggar, Algeria). *Journal of Petrology*, **44,** 517–545.

Pattison, D. R. M. & Begin, N. J., 1994. Zoning patterns in orthopyroxene and garnet in granulites: implications for geothermometry. *Journal of Metamorphic Geology*, **12,** 387–410.

Pattison, D. R. M., Chacko, T., Farquhar, J. & McFarlane, C. R. M., 2003. Temperatures of granulite-facies metamorphism: constraints from experimental phase equilibria and thermobarometry corrected for retrograde exchange. *Journal of Petrology*, **44,** 867–900.

Pimentel, M. M., Fuck, R. A., Jost, H., Ferreira Filho, C. F. & Araujo, S. M., 2000. The basement of the Brasília Fold Belt and the Goiás Magmatic Arc. In: *Tectonic Evolution of South America* (eds Cordani, U., Milani, E., Thomaz Filho, A. & Campos, D.), pp. 195–229. 31st International Geological Congress, Rio de Janeiro.

Pimentel, M. M., Filho, C. F. F. & Armstrong, R., 2004. SHRIMP U–Pb and Sm–Nd ages of the Niquelandia layered complex: Meso- (1.25 Ga) and Neoproterozoic (0.79 Ga) extensional events in central Brazil. *Precambrian Research*, **132,** 133–153.

Piuzana, D., Pimentel, M. M., Fuck, R. A. & Armstrong, R., 2003. Neoproterozoic granulite facies metamorphism and coeval granitic magmatism in the Brasília Belt, Central Brazil: regional implications of new SHRIMP U–Pb and Sm–Nd data. *Precambrian Research*, **125,** 245–273.

Powell, R. & Holland, T. J. B., 1988. An internally consistent dataset with uncertainties and correlations; 3, Applications to geobarometry, worked examples and a computer program. *Journal of Metamorphic Geology*, **6,** 173–204.

Powell, R. & Sandiford, M. A., 1987. Sapphirine and spinel phase relations in the system $FeO–MgO–Al_2O_3–SiO_2–TiO_2–O_2$ in the presence of quartz and hypersthene. *Contributions to Mineralogy and Petrology*, **98,** 64–71.

Powell, R., Holland, T. J. B. & Worley, B., 1998. Calculating phase diagrams involving solid solutions via non-linear equations, with examples using THERMOCALC. *Journal of Metamorphic Geology*, **6,** 173–204.

Powell, R., Guiraud, M. & White, R. W., 2005. Truth and beauty in metamorphic phase-equilibria: conjugate variables and phase diagrams. *Canadian Mineralogist*, **43,** 21–33.

Raith, M., Karmakar, S. & Brown, M., 1997. Ultra-high-temperature metamorphism and multistage decompressional evolution of sapphirine granulites from the Palni Hill Ranges, southern India. *Journal of Metamorphic Geology*, **15,** 379–399.

Sajeev, K. & Osanai, Y., 2004. Ultrahigh-temperature metamorphism (1150 °C, 12 kbar) and multistage evolution of

Mg–Al-rich granulites from the Central Highland Complex, Sri Lanka. *Journal of Petrology*, **45,** 1821–1844.

Sajeev, K., Osanai, Y. & Santosh, M., 2004. Ultrahigh-temperature metamorphism followed by two-stage decompression of garnet–orthopyroxene–sillimanite granulites from Ganguvarpatti, Madurai block, southern India. *Contributions to Mineralogy and Petrology*, **148,** 26–46.

Sandiford, M. & Powell, R., 1991. Some remarks on high-temperature–low-pressure metamorphism in convergent orogens. *Journal of Metamorphic Geology*, **9,** 333–340.

Thompson, P., Harley, S. L. & Carrington, D. P., 2001. H_2O–CO_2 partitioning between fluid, cordierite and granitic melt at 5 kbar and 900 °C. *Contributions to Mineralogy and Petrology*, **142,** 107–118.

Tinkham, D. K., Zuluaga, C. A. & Stowell, H. H., 2001. Metapelitic phase equilibria modeling in MnNCKFMASH: the effect of variable Al_2O_3 and MgO/(MgO + FeO) on mineral stability. *Geological Materials Research*, **3,** 1–42.

White, R. W. & Powell, R., 2002. Melt loss and the preservation of granulite facies mineral assemblages. *Journal of Metamorphic Geology*, **20,** 621–632.

White, R. W., Powell, R. & Holland, T. J. B., 2001. Calculation of partial melting equilibria in the system Na_2O–CaO–K_2O–FeO–MgO–Al_2O_3–SiO_2–H_2O (NCKFMASH). *Journal of Metamorphic Geology*, **19,** 139–153.

White, R. W., Powell, R. & Clarke, G., 2002. The interpretation of reaction textures in Fe-rich metapelitic granulites of the Musgrave Block, central Australia: constraints from mineral equilibria calculations in the system K_2O–FeO–MgO–Al_2O_3–SiO_2–H_2O–TiO_2–Fe_2O_3. *Journal of Metamorphic Geology*, **20,** 41–55.

Yardley, B. W. D. & Valley, J. W., 1997. The petrologic case for a dry lower crust. *Journal of Geophysical Research*, **102,** 12173–12186.

Received 21 December 2004; revision accepted 20 May 2005.